



Perceptual decision making: Biases in post-error reaction times explained by attractor network dynamics

Kevin Berlemont, Jean-Pierre Nadal

► To cite this version:

Kevin Berlemont, Jean-Pierre Nadal. Perceptual decision making: Biases in post-error reaction times explained by attractor network dynamics. 2018. hal-01718366v2

HAL Id: hal-01718366

<https://hal.science/hal-01718366v2>

Preprint submitted on 20 Apr 2018 (v2), last revised 20 Nov 2018 (v4)

HAL is a multi-disciplinary open access archive for the deposit and dissemination of scientific research documents, whether they are published or not. The documents may come from teaching and research institutions in France or abroad, or from public or private research centers.

L'archive ouverte pluridisciplinaire **HAL**, est destinée au dépôt et à la diffusion de documents scientifiques de niveau recherche, publiés ou non, émanant des établissements d'enseignement et de recherche français ou étrangers, des laboratoires publics ou privés.

Perceptual decision making: Biases in post-error reaction times explained by attractor network dynamics

Kevin Berlemont¹, and Jean-Pierre Nadal^{1, 2}

¹ Laboratoire de Physique Statistique, École Normale Supérieure, PSL University, Université Paris Diderot, Université Sorbonne Paris Cité, Sorbonne Université, CNRS, 75005 Paris, France.

² Centre d'Analyse et de Mathématiques Sociales, École des Hautes Études en Sciences Sociales, PSL University, CNRS, 75006 Paris, France.

Abstract Perceptual decision-making is the subject of many experimental and theoretical studies. Whereas most modeling analyses are based on statistical processes of accumulation of evidence, less attention is being devoted to the modeling with attractor network dynamics, even though they describe well psychophysical and neurophysiological data. In particular, very few works confront attractor models' predictions with data from continuous sequences of trials.

Recently however, numerical simulations of a biophysical competitive attractor network model have shown that such network can describe sequences of decision trials and reproduce repetition biases observed in perceptual decision experiments. Here we get more insights into such effects by considering an extension of the reduced attractor network model of Wong and Wang (2006), taking into account an inhibitory current delivered to the network once a decision has been made. We make explicit the conditions on this inhibitory input for which the network can perform a succession of trials, without being either trapped in the first reached attractor, or losing all memory of the past dynamics. We study in details the reaction times properties during a sequence of decision trials. Quite remarkably, we show that, in the absence of any feedback about the correctness of the decision, the network exhibits, qualitatively and with the correct orders of magnitude, post-error slowing and post-error improvement in accuracy, two subtle effects observed in behavioral experiments. Our work thus provides evidence that such effects result from intrinsic properties of the neural decision dynamics.

Introduction

Typical experiments on perceptual decision-making consist of series of successive trials separated by a short time interval, in which performance in identification and reaction times are measured. The most studied protocol is the one of Two-Alternative Forced-Choice (TAFC) Task – see e.g. Ratcliff (1978); Laming (1979b); Vickers (1979); Townsend and Ashby (1983); Busemayer and Townsend (1993); Shadlen and Newsome (1996); Usher and McClelland (2001); Ratcliff (2004). Several studies have demonstrated strong serial dependence in perceptual decisions between temporally close stimuli (Fecteau and Munoz, 2003; Danielmeier and Ullsperger, 2011; Jentzsch and Dudschig, 2009). Such effects have been studied in the framework of statistical models of accumulation of evidence (Dutilh et al., 2011), the most common theoretical approach to perceptual decision-making, see e.g. Ratcliff (1978); Ashby (1983); Shadlen et al. (2006); Ratcliff and McKoon (2008); Bogacz (2009).

Wang (2002) proposed an alternative approach to the modeling of perceptual decision making based on a biophysical cortical network model of leaky integrate-and-fire (LIF) neurons. The model is shown to account for the random dot experiments results of Shadlen and Newsome (2001) and Roitman and Shadlen (2002). This decision-making attractor network has been first studied in the context of a task requiring to keep in memory the last decision. This working memory effect is precisely achieved by having the network activity trapped into an attractor state. However, in the context of consecutive trials, the neural activities have to be reset in a low activity state before the onset of the next stimulus. Bonaiuto et al. (2016) have considered a parameter range of weaker excitation where the working memory phase is suppressed. The main result is that the performance of the network is biased towards the previous decision, an effect which decreases with the inter-trials time. Due to the slow relaxation dynamics in the model, the authors only study inter-trial times longer than 1.5 s. However, sequential effects have been reported for shorter inter-trial times, such as 512 ms in Laming (1979b) or even 200 ms in Danielmeier

and Ullsperger (2011).

Instead of decreasing the recurrent excitation, an alternative is to introduce an additional inhibitory input following a decision (Lo and Wang, 2006; Engel et al., 2015; Bliss and DEsposito, 2017). Lo and Wang (2006) have proposed such a mechanism to account for the control of the decision threshold. However, they do not study the model behavior in the context of sequences of trials. Gao et al. (2009) have proposed a more complex attractor network with specific memory units implementing a biasing mechanism directly into the network architecture.

The purpose of the present paper is to revisit this issue of dealing with sequences of successive trials within the framework of attractor networks as introduced by Wang (2002), with a focus on inter-trial times as short as 200 ms. We do so by taking advantage of the reduced model proposed by Wong and Wang (2006). This model consists of an effective network of only two units, representing the pool activities of two populations of cells, each one being specific to one of the two stimulus categories. Wong and Wang (2006) derive the equations of the reduced model and choose the parameters values in order to preserve as much as possible the dynamical and behavioral properties of the original full model. Thanks to this reduction, one can then perform a detailed mathematical analysis.

In line with Lo and Wang (2006), we take into account an inhibitory current originating from the basal ganglia, occurring once a decision has been made. We explore the serial dependence effects predicted by the model and compare with empirical findings. Beside the expected decision bias toward the previous decision, our main finding is that, without any fine tuning of parameters, the model reproduces two main post-error adjustments in the absence of feedback on the correctness of the decision: post-error slowing (PES) and post-error improvement in accuracy (PIA), PES consisting of longer reaction times, and PIA of smaller error rates, for trials following a trial with incorrect decision.

Materials and Methods

We are interested in modeling experiments where a subject has to decide whether a stimulus belongs to one or the other of two categories, hereafter denoted L and R . A specific example is the one of random dot experiments (Roitman and Shadlen, 2002; Shadlen and Newsome, 2001), where a monkey performs a motion discrimination task in which it has to decide whether a motion direction, embedded into a random dot motion, is towards left (L) or right (R). We consider a decision-making recurrent network of spiking neurons governed by local excitation and feedback inhibition, as introduced and studied in Compte et al. (2000) and Wang (2002). Since mathematical analysis cannot be performed for such complex networks, one must rely on simulations which, themselves, can be computationally heavy. For our analysis, we make use of the reduced firing-rate model of Wong and Wang (2006) obtained by a systematic reduction, within a mean-field approach, of the detailed biophysical attractor network model. Since this model has been built to reproduce as faithfully as possible the neural activity of the full spiking neural network, it can be used as a proxy for simulating the full spiking network (Engel and Wang, 2011; Engel et al., 2015). Here, we also make use of this model to gain better insights into the understanding of the model behavior. In particular, one can conveniently represent the network dynamics in a 2-d phase plane and analyze the network dynamics (Wong and Wang, 2006).

A reduced recurrent network model for decision-making.

We consider the model architecture illustrated in Fig. 1, which consists of two competing units, each one representing an excitatory neuronal pool, selective to one of the two categories, L or R . The two units inhibit one another, while they are subject to self-excitation. The dynamics is described by a set of coupled equations for the synaptic activities S_L and S_R of the two units L and R – see the Appendix in Wong and Wang (2006) for more details –:

$$i \in \{L, R\}, \quad \frac{dS_i}{dt} = -\frac{S_i}{\tau_S} + (1 - S_i) \gamma f(I_{i,tot}) \quad (1)$$

The synaptic drive S_i for pool $i \in \{L, R\}$ corresponds to the fraction of activated NMDA conductance, and $I_{i,tot}$ is the total synaptic input current to unit i . The function f is the effective single-cell input-

output relation (Abbott and Chance, 2005), giving the firing rate as a function of the input current:

$$f(I_{i,tot}) = \frac{aI_{i,tot} - b}{1 - \exp[-d(aI_{i,tot} - b)]} \quad (2)$$

where a, b, d are parameters whose values are obtained through numerical fit.

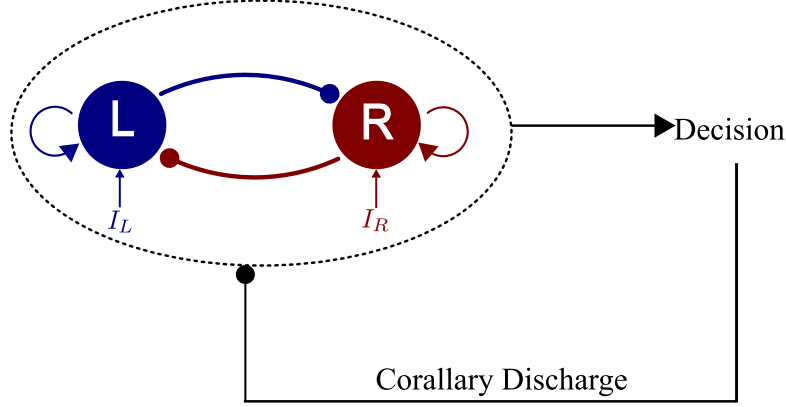


Figure 1: Architecture of the extended two-variables model. *Reduced two-variable model constituted of two neural units, endowed with self-excitation and effective mutual inhibition. The extension consists of the addition of the corollary discharge originating from the basal ganglia, an inhibitory input onto both units occurring just after a decision is made.*

The total synaptic input currents, taking into account the inhibition between populations, the self-excitation, the background current and the stimulus-selective current can be written as:

$$I_{L,tot} = J_{L,L}S_L - J_{L,R}S_R + I_{stim,L} + I_{noise,L} \quad (3)$$

$$I_{R,tot} = J_{R,R}S_R - J_{R,L}S_L + I_{stim,R} + I_{noise,R} \quad (4)$$

with $J_{i,j}$ the synaptic couplings. The minus signs in the equations make explicit the fact that the inter-units connections are inhibitory (the synaptic parameters $J_{i,j}$ being thus positive or null). The term $I_{stim,i}$ is the stimulus-selective external input. If μ_0 denotes the strength of the signal, the form of this stimulus-selective current is:

$$I_{stim,i} = J_{A,ext}\mu_0 \left(1 \pm \frac{c}{100\%}\right) \quad (5)$$

with $i = L, R$. The quantity c is the coherence level of the stimulus (equivalently $1 - c/100$ quantifies the ambiguity of the stimulus). In the random dot motion framework, it corresponds to the percent of dots contributing to the coherent motion. It gives the strength of the signal bias, positive when the stimulus favors population L , negative in the other case. Following Wang (2002), this input forms the pooling of the activities of middle temporal neurons firing according to their preferred directions. This input current is only present during the presentation of the stimulus and is shut down once the decision is made.

In addition to the stimulus-selective part, each unit receives individually an extra noisy input, fluctuating around the mean effective external input I_0 :

$$\tau_{noise} \frac{dI_{noise,i}}{dt} = -(I_{noise,i}(t) - I_0) + \eta_i(t) \sqrt{\tau_{noise}} \sigma_{noise} \quad (6)$$

with τ_{noise} a synaptic time constant which filter the white-noise. For the simulations, unless otherwise stated parameters values will be those of Table 1.

Initially the system is at a symmetric state, with low firing rates and synaptic activities (see Figure 1-1). On the presentation of the stimulus, the system evolves towards one of the attractor states, corresponding to the decision state. In these attractors, the 'winning' unit fires at a higher rate than the other. We are interested in reaction time experiments. In our simulations, we consider that the system has made a decision when for the first time the firing rate of one of the two units crosses a threshold θ , fixed

Parameter	Value	Parameter	Value
a	270 Hz/nA	σ_{noise}	0.02 nA
b	108 Hz	τ_{noise}	2 mS
d	0.154 s	I_0	0.3255 nA
γ	0.641	μ_0	30 Hz
τ_S	100 ms	$J_{A,ext}$	5.2×10^{-4} nA. Hz ⁻¹
$J_{N,LL} = J_{N,RR}$	0.2609 nA	$J_{N,LR} = J_{N,RL}$	0.0497 nA
θ	20 Hz		
$I_{CD,max}$	0.035 nA	τ_{CD}	200 ms

Table 1: Numerical values of the model parameters: above the dashed line, as taken from Wong and Wang (2006); below the dashed line, values of the additional parameters specific to the present model (see text).

here at 20 Hz. We have chosen this parameter value, slightly different from the one in Wong and Wang (2006), from the calibration of the extended model discussed below on sequential decision trials with short response-stimulus intervals. We have checked that this does not affect the psychometric function of the network (see Figure 1-2).

Extended version: inhibitory corollary discharge

Studies like Roitman and Shadlen (2002) show that, during decision tasks, neurons activity experiences a decay following the responses. The prefrontal cortex-basal ganglia-thalamic circuit (BG) plays a fundamental role in many cognitive functions including perceptual decision-making (see Wei and Wang (2016)), inhibitory control and working memory. The BG circuit has been studied as providing a mechanism for modulating the decision threshold in reaction time tasks in Lo and Wang (2006). The authors introduce an extension of the biophysical model of Wang (2002) consisting in modeling the coupling between the network, the basal ganglia and the superior colliculus. The net effect is an inhibition onto the populations in charge of making the decision. The authors show that the decision threshold is signaled by an all-or-none inhibitory burst response towards the cortical neurons, a corollary discharge (CD) (Crapse and Sommer, 2009). While Lo and Wang (2006) address the issue of the control of the decision threshold, they do not discuss the relaxation dynamics induced by the corollary discharge, nor the effects on sequential decision tasks. The study of serial dependence making use of the inhibitory corollary discharge has been done for a ring model of visual working memory in (Bliss and DEsposito, 2017), and in the context of learning (Engel et al., 2015).

In order to analyze these effects with the reduced attractor network model, we assume that, after crossing the threshold, the network receives an inhibitory current, mimicking the joint effect of basal-ganglia and superior colliculus on the two neural populations (Figure 1). The modification of the excitatory weights (as in Bonaiuto et al. (2016)) is briefly investigated in Figure 1-3.

In the specific case of Engel et al. (2015), the function of the corollary discharge is to reset neural activity in order to allow the network to learn during the next trial. For this, the form of the CD input is chosen as a constant inhibitory current during a period of 300ms. Within our model, such strong input would lead to a reset to the resting state with no memory of the previous trial. We thus rather consider here a smooth version of this discharge, assuming an input current with a standard exponential form (Finkel and Redman, 1983). The inhibitory input originating from the basal ganglia, $I_{CD}(t)$, is then given by:

$$I_{CD}(t) = \begin{cases} 0 & \text{during stimulus presentation} \\ -I_{CD,max} \exp(-(t - t_D)/\tau_{CD}) & \text{after the decision time, } t_D \end{cases} \quad (7)$$

The relaxation time constant τ_{CD} is chosen in the biological range of synaptic relaxation times and in accordance with the relaxation-times range of the attractor (see Table 1-1), $\tau_{CD} = 200$ ms. Therefore

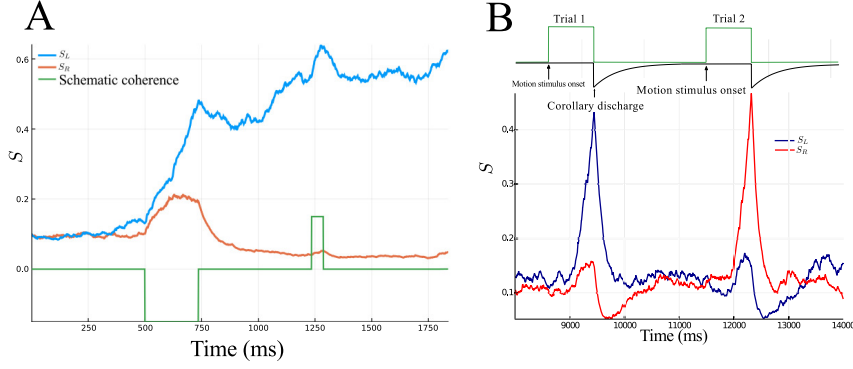


Figure 2: Time course of synaptic activities. (A) The green curve represents, schematically, the onset of the stimulus with the sign of the bias (coherence). In this simulation, $I_{CD,max} = 0.01$ nA and the model is not able to perform sequential decision-making. The blue and orange curve correspond to the activities of the units. During the resting time, the previous attractor state is not left. (B) The upper part corresponds to a schematic time course of the input signal and of the corollary discharge. The input signal (green) corresponds to the sensory information acquired during the task, and the control signal (black) to the corollary discharge from basal ganglia onto the network. Here, we take $I_{CD,max} = 0.035$ nA. The lower part represents the time course of the neural activities S_L and S_R in the model. The first stimulus leads to the choice R, and we observe the decay following response. This allows the network to make the opposite choice, L, for the second stimulus.

the input currents are modified as follows:

$$I_{L,tot}(t) = J_{LL}S_L(t) - J_{L,R}S_R(t) + I_{stim,L}(t) + I_{noise,L}(t) + I_{CD}(t) \quad (8)$$

$$I_{R,tot}(t) = J_{RR}S_R(t) - J_{R,L}S_L(t) + I_{stim,R}(t) + I_{noise,R}(t) + I_{CD}(t). \quad (9)$$

In Fig. 2 we illustrate the network dynamics between two consecutive stimuli during a sequence of trials, for two different values of the corollary discharge. We also make use of non-linear dynamical tools to analyze the network dynamics. In Fig. 3 we illustrate how the corollary discharge following a response modifies the energy landscape (potential well in which the system evolves) with respect to the original model with no CD. If the inhibitory current following the decision is too weak, the network behaves as in the absence of this current. Namely, the network is not able to make a new decision different from the previous one (Figure 2.A). Even when the opposite stimulus is presented, the system cannot leave the attractor previously reached, unless in presence of unrealistic strong biases. If however the strength $I_{CD,max}$ is strong enough, the corollary discharge makes the system to escape from the previous attractor and to relax towards the neutral resting state with low firing rates. If too strong, or in case of a too long RSI, at the onset of the next stimulus the neutral state has been reached and memory of past trials is lost. For an intermediate range of parameters, at the onset of the next stimulus the system has escaped from the attractor but is still on a trajectory dependent on the previous trial (Figure 2.B).

With the inhibitory corollary discharge, after the threshold is crossed by one of the two neural populations, there is thus big drop in the neuronal activity, corresponding to the exit from the previous attractor state. This type of time-course is in agreement with the experimental findings of Roitman and Shadlen (2002) who measure the activity of LIP neurons during a decision task. During the resting time, the amount by which the activities decay determines the initial neural state at the onset of the new stimulus, leading thus to possible biases in the next decision.

Numerical simulations design and Statistical tests

Numerical simulations

In Figure 4 we give a schematic representation of a simulation of sequential decision-making. Each orange rectangle corresponds to a stimulus, with a random value of coherence in the desired range. The stimulus is present until a decision is made. The set of dynamical equations (1,6) – with the definitions (2,5,7,8,9) – is integrated using Euler-Maruyama method with a time step of 0.5 ms. At the beginning of

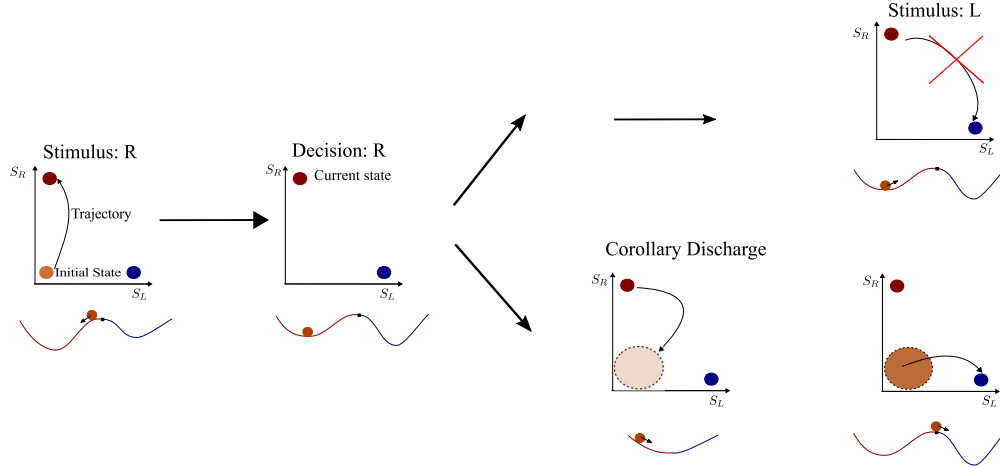


Figure 3: Phase-plane analysis of sequential decision making: Neural dynamics between two consecutive stimuli, represented in the phase-plane, together with the corresponding energy landscape. The red color corresponds to the attractor R , and the blue to attractor L . The first two schema (Left) illustrates the dynamics from the stimulus presentation to the time of decision. Right, upper panel: dynamics for the original reduced model (no corollary discharge). Right, bottom: dynamics in the model with strong enough corollary discharge.

a simulation, the system is set in a symmetric state $S_L = S_R = s_0$, with low firing rates and synaptic activities, $s_0 = 0.1$. We compute the instantaneous population firing rates, or the synaptic dynamical variables S_L and S_R , by averaging on a time window of 2 ms, slided with a time step of 1 ms. The accuracy of the network's performance is defined as the percentage of trials in which the units crossing the threshold corresponds to the stronger input. For data analysis we mainly work with the variables S_L and S_R which are analog to the firing rates of the neuron, but give less noisy figures. We consider that the system has made a decision when for the first time the firing rate of one unit crosses a threshold θ , fixed at 20 Hz. The reaction time during one trial is defined as the time needed for the network to reach the threshold from the start of the input stimulus. We neglect the possible additional time due to motor reaction.

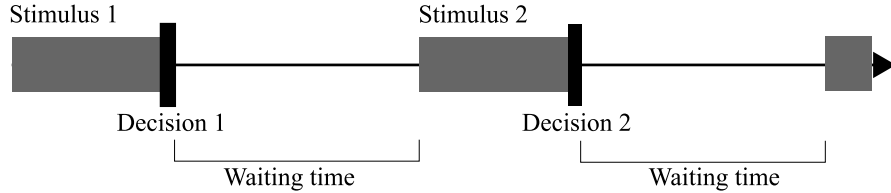


Figure 4: Simulations protocol. The time-sketch of the simulations can be decomposed into a succession of identical blocks. Each block, corresponding to one trial, consists of: the presentation of a stimulus with a randomly chosen coherence (gray box), a decision immediately followed by the removal of the stimulus, a waiting time of constant duration corresponding to the RSI.

We list in Table 1 the model parameters which correspond to the one of the simulations. For Figure 5 and 7 we have used continuous sequences of 10000 trials and for the Figures 8-14 it was sequences of 1000 trials averaged on 50 participants.

Statistical tests

Following Benjamin et al. (2018), we consider a p-value of 0.005 as a criterion for rejecting the null hypothesis in a statistical test. To assess if the distributions of two continuous variables are different, we make use of the Kolmogorov-Smirnov test (Hollander et al., 2014), and in the case of discrete distributions we use the Anderson-Darling test (Shorack and Wellner, 2009). For very large samples, we

use the energy distance (Rizzo and Székely, 2016), which is a metric distance between the distributions of random vectors. We use the associated E-statistic (Szekely and Rizzo, 2013) for testing the null hypothesis that two random variables X and Y have the same cumulative distribution functions. For testing whether the means of two samples are different we make use of the Unequal Variance test (Welch's test) (Hollander et al., 2014).

Softwares and Code accessibility

For the simulations we made use of the Julia language (Bezanson et al., 2014). The code of the simulations can be obtained from the corresponding author upon request. We made use of the XPP software (Ermentrout and Mahajan, 2003) for the phase-space analysis and the computation of the relaxation time constant of the dynamical system. Figures 8, 9, 10 and 11 were realized using Python and the other are in the same language as the simulations. The E-statistics tests were performed using the R-Package: *energy package* (Rizzo and Székely, 2014).

Results

Sequential dynamics and choice repetition biases

The qualitative dynamical properties described above, namely the two populations neural dynamics before a decision, followed by the relaxation after decision before the onset of the next stimulus, provide the internal dynamical properties at the origin of sequential effects. This mechanism is described in Bonaiuto et al. (2016) for the analysis of sequence repetition biases. In the present model, although the mechanism is qualitatively the same, the relaxation is induced by the corollary discharge. This results in different quantitative properties, notably in the time scale of the relaxation. Quite importantly, we will show later that these same dynamical properties explain as well post-error adjustments. As a preliminary step, it is thus necessary to describe more precisely the inter trial dynamics. We do so by exploring response repetition bias, as studied in Bonaiuto et al. (2016), and confronting with empirical findings.

In all the following, we explore the model properties in function of the two main parameters, the amplitude of the corollary discharge, $I_{CD,max}$, and the duration of the response-stimulus interval (RSI), that is the time between the response of the subject and the presentation of the next stimulus (in our model the time at which the decision threshold is reached).

Network behavior: Reaction times biases

We run a simulation of 10000 consecutive trials, each of them with a coherence value randomly chosen between 12 values in the range $[-20, 20]$. We do so for two values of the corollary discharge amplitude, $I_{CD,max} = 0.035$ nA and $I_{CD,max} = 0.06$ nA, with a RSI of 1.5 s, the other parameters being given on Table 1. We analyze the effects of response repetition by separating the trials into two groups depending on whether the decisions made on the previous and on the current trials are identical or different, hereinafter referred to as *Repeated* and *Alternated* cases, respectively. We find that the distribution of coherence values are identical for the two groups, for both values of $I_{CD,max}$ (Anderson-Darling test, $p = 0.77$ and $p = 0.82$ respectively). We study the reaction times separately for the two groups, and present the results in Figure 5.

In Figure 5.C we represent the so called energy distance (Rizzo and Székely, 2016; Székely and Rizzo, 2013) between the repeated and alternated reaction times distribution. As we can observe, the distance decreases, hence the sequential effect diminishes, as the corollary discharge amplitude $I_{CD,max}$ increases. For the specific case of Figures 5.A and B, the corresponding E-statistic for testing equal distributions leads to the conclusion that in the case $I_{CD,max} = 0.035$ nA, the two reaction-time distributions are different ($p = 0.0019$). This implies that the behavior of the network is influenced by the previous trial, and we observe a faster reaction time (around 70 ms) when the choice is repeated (Figure 5A). On the contrary, for $I_{CD,max} = 0.06$ nA (Figure 5.B), the two histograms cannot be distinguished (E-statistic test, $p = 0.25$).

We have checked that increasing the RSI has a similar effect to increasing the corollary discharge amplitude (see Figure 5-1). We observe sequential effects for RSI values in the range 1.5 to 5 seconds,

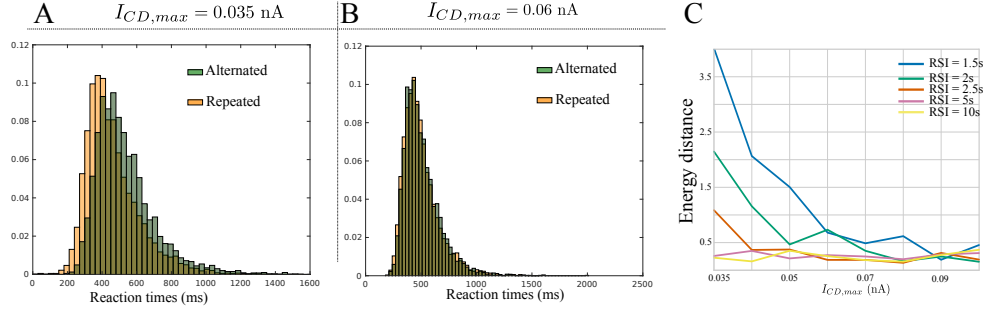


Figure 5: Histogram of the reaction times. We run simulations at (A) $I_{CD,max} = 0.035$ nA and (B) $I_{CD,max} = 0.06$ nA, with a RSI of 1.5 second. The green histogram corresponds to the Alternated case, that is when the decisions made at the n th and $n+1$ trials are different. The orange histogram corresponds to the Repeated case, that is when the decisions made at the n th and $n+1$ trials are identical. (C) Energy distance between the repeated and alternated histograms. The x-axis represents the strength of the corollary discharge, and the color code the duration of the RSI in seconds.

in accordance with psychological experiments, where such effects are observed for RSI less than 5 seconds (Laming, 1979b; Rabbitt and Rodgers, 1977; Bonaiuto et al., 2016).

Neural correlates: Dynamics analysis

With the relaxation of the activities induced by the corollary discharge, the state of the network at the onset of the next stimulus lies in-between the attractor state corresponding to the previous decision, and the neutral attractor state. When averaging separately over repeated and alternated trials, we find, as detailed below, that this relaxation dynamics has different behaviors depending on whether the next decision is identical or different from the previous one. Note that this is a statistical effect which can only be seen by averaging over a very large number of trials.

In Figure 6 we compare two examples of network activity, one with an alternated choice, and one with a repeated choice, by plotting the dynamics during two consecutive trials. We observe in Figure 6.A, the alternated case, that previous to the onset of the second stimulus (light blue rectangle) the activities of the two populations are at very similar levels. In contrast, for the case of a repeated choice, Figure 6.C, the activities are well separated, with higher firing rates.

In Figure 6.B and D we represent the dynamics of the network in the phase-plane diagram. We show in Figure 6.D the phase-plane's dynamic in the case of a repeated choice (trajectory in blue). On this same panel, for comparison we reproduce in light red the dynamics, shown in Figure 6.B, during the first trial in the alternated case. We observe that the relaxation between trials is different in the two cases. As can be seen in Figure 6.D, the network states at the time of decision are different depending on whether the network makes a decision identical to, or different from, the one made at the previous trial.

In order to check the statistical significance of these observations, we represent in Figure 7 the mean activities during the RSI, obtained by averaging the dynamics over all trials, separately for the alternated and repeated groups. As expected, for small values of $I_{CD,max}$ (0.035 nA), the two dynamics are clearly different. This difference diminishes during relaxation. However at the onset of the next stimulus we can still observe some residues, statistically significant according to an Anderson-Darling test done on the 500 ms prior to the next stimulus (between winning population, $p = 0.0034$, between losing population $p = 3.2 \times 10^{-8}$).

Those differences in the relaxation dynamics are characteristic of the sequential effects, but they are not the explication of the choice repetition biases. Looking at Figure 7.A, we observe that the ending points of the alternated and repeated relaxations are biased with respect to the symmetric state. At the beginning of the next stimulus the network is already in the basin of attraction of the repeated case. Hence, it will be harder to reach the alternated attractor stated (in the green region). When increasing $I_{CD,max}$ (Figure 7.B), we observe that the ending state of the relaxation is closer to the attractor state. Hence, the biases in sequential effects disappear because at the beginning of the next stimuli the network starts from a symmetric state.

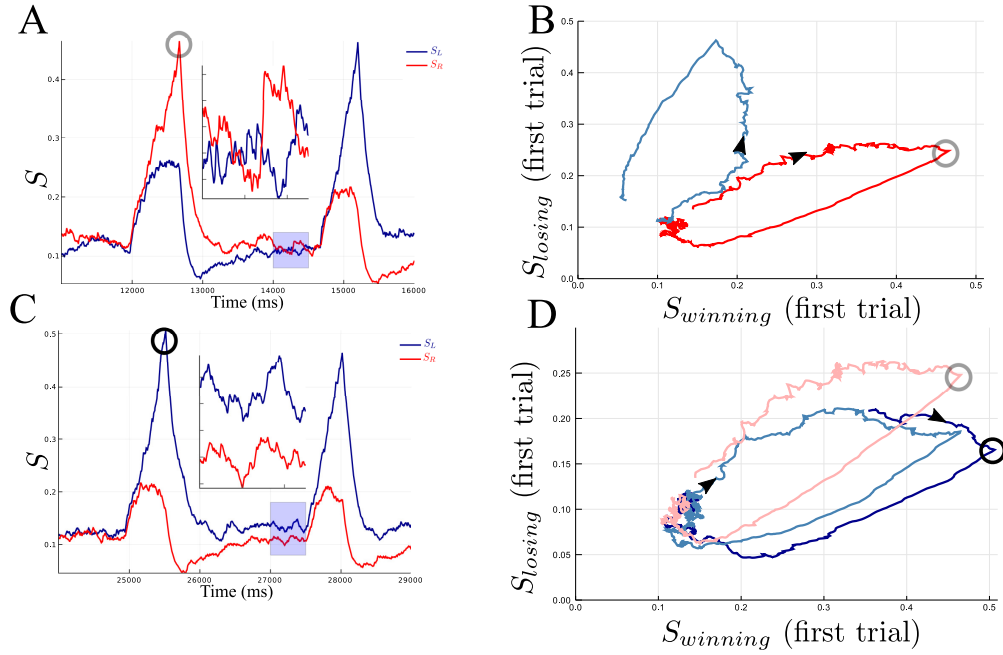


Figure 6: Network activity during two consecutive trials. Panels (A) and (B) represent the alternated case where the decision made is R then L, and panels (C) and (D) represent the case where decision L is made and repeated. Panels (A) and (C) plot the time course activities of the network. The light blue zone is zoomed in order to better see the dynamics just before the onset of the second stimulus. The red and blue curves correspond to the activities of, respectively, the R and L network units. Panels (B) and (D) represent, respectively, the (A) and (C) dynamics in the phase-plane coordinates. On panel (B) the dynamics evolves from dark red (first trial) to light blue (2nd trial), and on panel (D) from dark blue (first trial) toward light blue (2nd trial). The gray – respectively black – circles identify a same specific point during the dynamics in panels (A) and (B) – resp. (C) and (D). In order to compare the alternated and repeated cases, (A,B) and (C, D), the dark red curve of panel (B), is reproduced on panel (D) giving the light red curve.

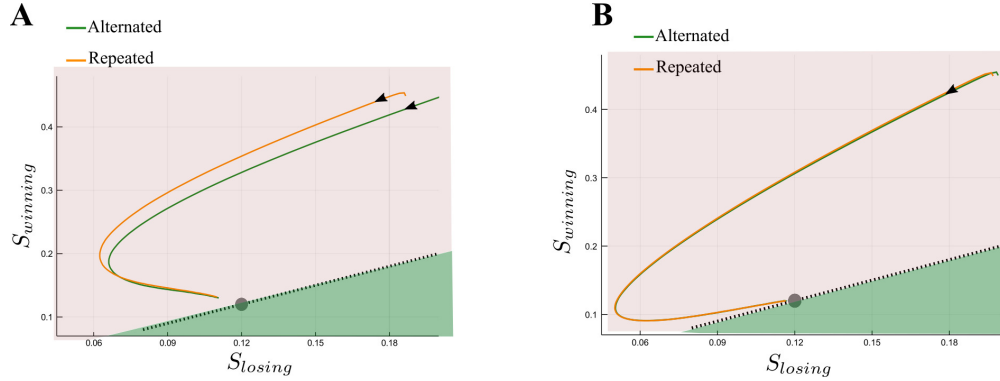


Figure 7: Phase plane analysis. Dynamics of the decaying activity between two successive trials, (A) for $I_{CD,max} = 0.035$ nA, and (B) for $I_{CD,max} = 0.06$ nA. The synaptic activity is averaged over all trials separately for each one of the two groups: alternated (green) and repeated (orange). The axis are $S_{winning}$ and S_{losing} (not S_R and S_L) corresponding to the mean synaptic activity of, respectively, the winning and the losing populations for this trial. Note the difference in scale of the two axes. The time evolution along each curve follows the black arrow. The dashed black line denotes the symmetric states ($S_L = S_R$) of the network, and the gray circle the neutral attractor. The shadow areas represent the basins of attraction (at low coherence levels) for the repeated and alternated trials, respectively pink and green.

To conclude this section, at the time of decision, the winning population has a firing rate higher than the losing population. After relaxation, at the onset of the next stimulus, they have more similar activities, but still sufficiently different for being away from the neutral attractor. This introduces a bias in favor of the more active population, that is the one corresponding to the previous decision. Reaction time will thus be shorter in case of a repetition.

On the contrary, for larger values of the inhibitory current, or longer RSI (see Figure 7-1), the dynamics are almost identical as can be seen in Figure 7 (Anderson-Darling test: between winning population, $p = 0.25$, between losing population $p = 0.4$), and both relaxation end near the neutral attractor state. The bias depending on the next stimulus is not observed anymore, and the sequential effect on reaction time hence disappear.

Post-error effect

Post-error slowing

Post-error slowing (PES) (Laming (1979b)) consists of prolonged reaction times in trials following an error, compared to reaction times following a correct trial. This effect has been observed in a variety of tasks: categorization (Jentzsch and Dudschig, 2009), flanker (Debener, 2005), Stroop (Gehring and Fencsik, 2001) tasks. Jentzsch and Dudschig (2009) and Danielmeier and Ullsperger (2011) found that the PES effect depends on the response-stimulus interval. The amplitude of this effect, defined as the difference between the mean reaction times, decreases as one increases the RSI, with values going from several dozens of milliseconds to zero. For RSI longer than 750 – 1500 ms, PES is not observed anymore.

In this section we investigate the occurrence of PES in our model, confronting the results to empirical findings. More specifically, we make numerical simulations in order to compare with the findings of Danielmeier and Ullsperger (2011). These authors considered a flanker task with stimuli belonging to one of two opposite categories (Left or Right directions). This protocol thus falls within the class of experiments that our model aims at describing. In the present work we test several coherence levels, each one leading to a different value of the error rate. In the experiments of Danielmeier and Ullsperger (2011), the ambiguity level is not quantified. However, the observed error rates are found around 10% which, within our model, corresponds to a coherence level of about $c = 10\%$. We will thus more specifically discuss this coherence level throughout the section. Finally, in Danielmeier and Ullsperger (2011), each subject performed a total number of 996 trials. In order to make simulations with a similar protocol, we compute the post-error effects for continuous session of 1000 trials.

In Figure 8.A we represent the phase diagram of the PES effect with respect to the coherence level (x -axis) and $I_{CD,max}$ (y -axis), at an intermediate RSI value of 500 ms. We first remark that there is three types of behaviors: post-error slowing effect (in red) / no effect on the reaction times (in gray) / post-error quickening (in blue). Figure 8.B zooms on a value of $I_{CD,max}$ for which PES occurs ($I_{CD,max} = 0.035$ nA). We observe that the magnitude of the PES effect goes from zero to ten milliseconds, hence remaining within the range of behavioral data (Jentzsch and Dudschig, 2009) (12 ms for a RSI of 1 second). The second remark concerns the variation of the PES effect with respect to the coherence level. In the region where we observe a PES effect, we find that it is enhanced under conditions when errors are infrequent. However, for large values of the coherence level, this effect cannot be observed anymore due to the absence of any error in the successive trials (almost 100% of correct trials). This occurrence of PES, principally at low error rates, has been found in experiments of Núñez Castellar et al. (2010); Notebaert et al. (2009), for which the authors observe PES when errors are infrequent, but not when errors are frequent.

In addition to PES, the model presents a domain in parameter space where reaction times are faster after an error than after a correct trial. We propose to call this effect *post-error quickening* (PEQ), as opposed to post-error slowing. Such effect is rarely mention in the literature. Hester et al. (2005) report post-error decrease in reaction time, but for aware errors and not for unaware errors. This seems in contradiction with Cohen (2009), who reports an increase of PES effect after aware errors. Hence, the experimental conditions for the observation of PEQ are not clearly specified. Our model, which exhibits PEQ at high coherence levels, thus provides predictions that could be tested. As shown in Figure 8.C, we find that this effect can occur or not along with PES, depending on the coherence level. Even if our model corresponds to situations where there is no feedback on the correctness of the answer, the fact that

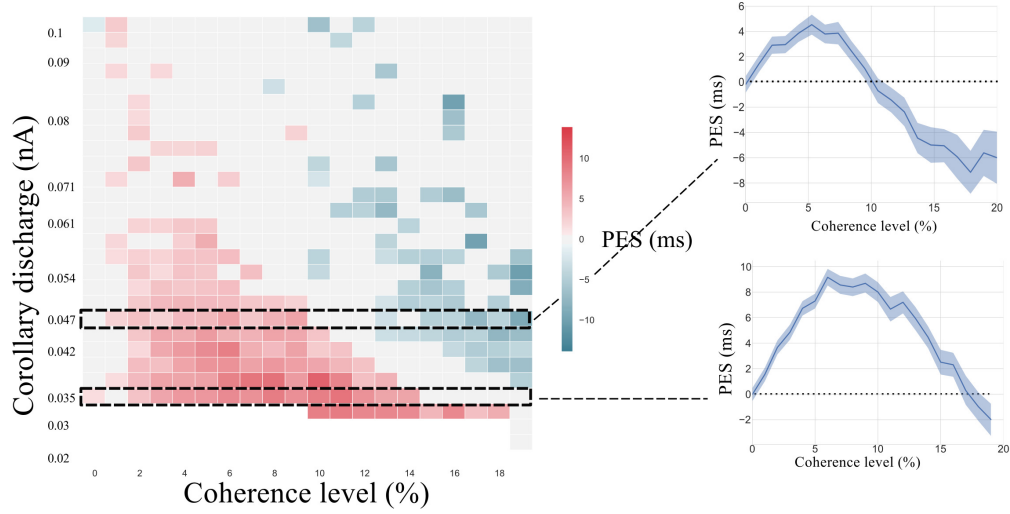


Figure 8: Post-error slowing. (A) Phase diagram of the PES effect at RSI of 500 ms. The bottom white zone corresponds to parameters where sequential decision-making is impossible. The red square corresponds to regions where PES is observed, and the blue ones where PEQ is observed (the darker the color, the stronger the effect). The black dashed squares correspond to specific regions where Panels B and C zoom. (B) PES effect (ms) with respect to the coherence level at $I_{CD,max} = 0.035$ nA. The light blue zone corresponds to the bootstrapped (Efron and Tibshirani, 1994) confidence interval at 95%. (C) PES effect (ms) with respect to the coherence level at $I_{CD,max} = 0.047$ nA. The light blue zone corresponds to the bootstrapped confidence interval at 95%.

PEQ occurs at high coherence levels may be seen as equivalent to cases with an aware error, since at high coherence level there is very few errors.

In behavioral experiments the PES effect depends strongly on the RSI. For RSI longer than 1000 – 1500 ms the observation or not of PES depends specifically on the decision task (Jentzsch and Dudschig, 2009; King et al., 2010). Despite the fact that PES is not always observed for long RSI, a common observation remains: if one keeps increasing the RSI, the PES effect eventually disappears. We investigate this behavior in the context of our network, by plotting the phase diagram at $I_{CD,max} = 0.035$ nA with respect to the RSI (Figure 9).

We observe that, for parameters where PES is observed at 500 ms, increasing the RSI leads to the weakening of the post-error slowing effect until its disappearance. At a RSI of 1600 ms (Figure 9.B) this effect is not present anymore, in agreement with experimental results (Jentzsch and Dudschig, 2009).

Post-error improvement in accuracy

Post-error improvement in accuracy (PIA) is another sequential effect reported in experiments (Laming, 1979b; Danielmeier and Ullsperger, 2011; Marco-Pallarés et al., 2008). PIA has been observed on different time-scales: long-term learning effects following error (Hester et al., 2005) and trial-to-trial adjustments directly after commission of error responses. We only consider this latter type of PIA. The specific conditions under which PIA can be observed in behavioral experiments have not been totally understood. We investigate this effect in the specific context of our model, the more the difference in accuracy is important the more this effect is considered as important.

In Figure 10 we represent the phase diagram of the PIA effect with respect to coherence levels (x-axis) and corollary discharge amplitude (y-axis). We denote a large region of parameters for which PIA is present. We find a magnitude of the PIA effect of about 2 – 4%, which is of the same order of magnitude as in the experiments where, for RSIs in the range 500 – 1000 ms, it is found that post-error accuracy is improved by approximatively 3% (Jentzsch and Dudschig, 2009).

Looking at Figure 10, the PIA and PES effects seem to be concomitant. However, if we zoom on specific regions (Figure 10.B and C), we can note some differences. The black dashed square regions correspond to the same parameters as in Figure 8. We first note that PIA is also observed in these regions.

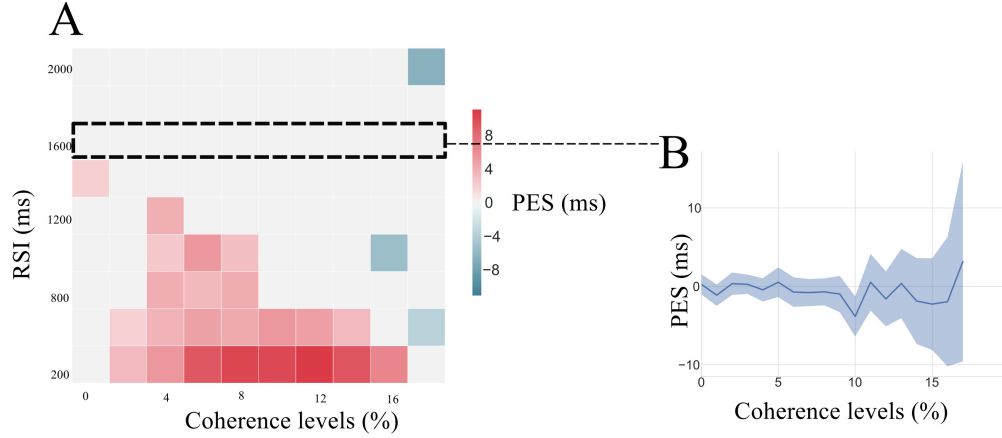


Figure 9: Post-error slowing depending on RSI. (A) Phase diagram of the PES effect at $I_{CD,max} = 0.035$ nA. The red square corresponds to regions where PES is observed (the darker the color, the stronger the effect). The black dashed squares correspond to a specific regions where panel B zooms. (B) PES effect (in ms) with respect to the coherence level at $I_{CD,max} = 0.035$ nA and at RSI of 1600 ms. The light blue zone corresponds to the bootstrapped confidence interval at 95%.

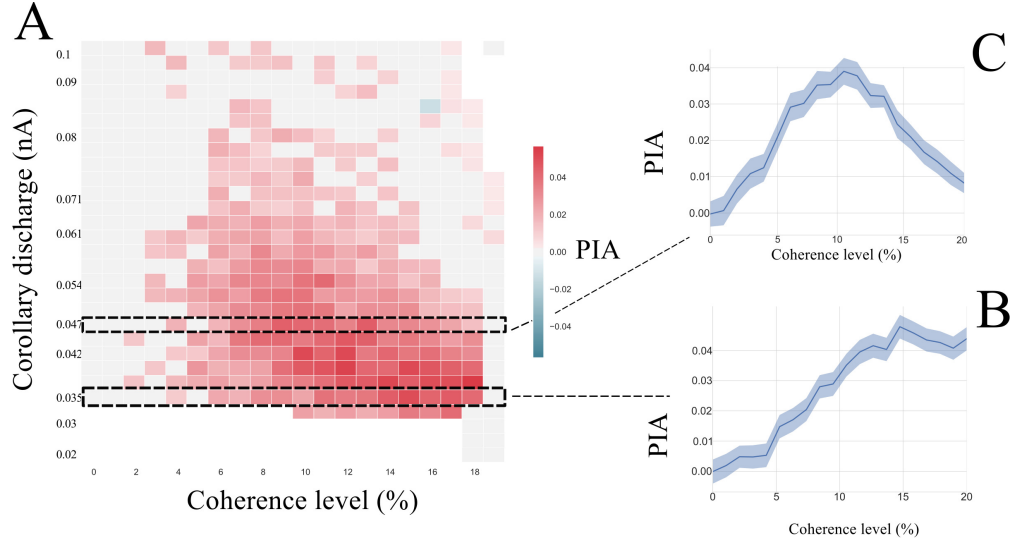


Figure 10: Post-error improvement in accuracy. (A) Phase diagram of the PIA effect at RSI of 500 ms. The bottom white zone corresponds to parameters where sequential decision-making is impossible. The red square corresponds to regions where PIA is observed. The black dashed squares correspond to specific regions where panels B and C zoom. (B) PIA effect with respect to the coherence level at $I_{CD,max} = 0.035$ nA. The light blue zone corresponds to the bootstrapped confidence interval at 95%. (C) PIA effect with respect to the coherence level at $I_{CD,max} = 0.047$ nA. The light blue zone corresponds to the bootstrapped confidence interval at 95%.

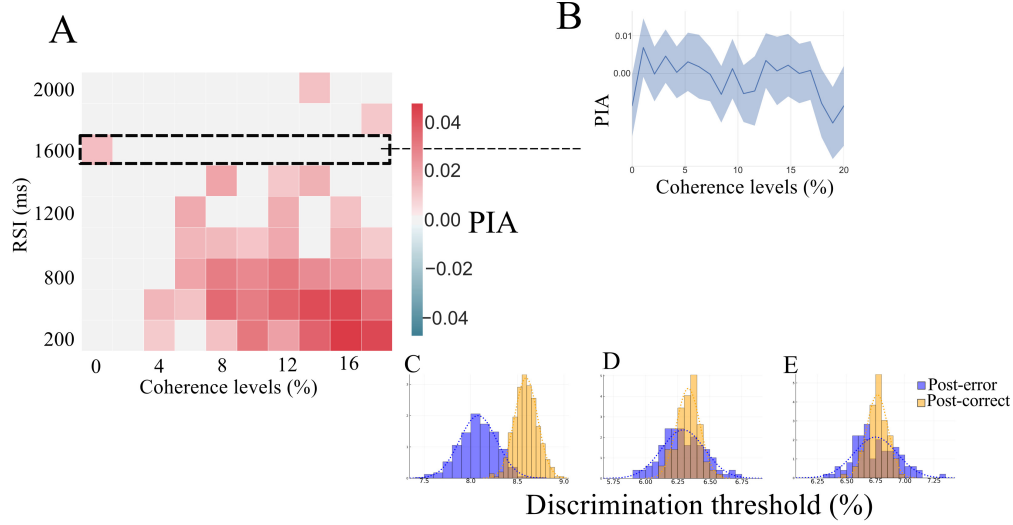


Figure 11: Post-error improvement in accuracy depending on RSI. (A) Phase diagram of the PIA effect at $I_{CD,max} = 0.035$ nA. The red square corresponds to regions where PIA is observed. The black dashed squares correspond to specific regions where panels B and C zoom. (B) PIA effect with respect to the coherence level at $I_{CD,max} = 0.035$ nA and a RSI of 1600 ms. The light blue zone corresponds to the bootstrapped confidence interval at 95%. (C)-(D)-(E) Distribution of the discrimination threshold for three values of RSI (500, 1000, 1500 ms respectively). In yellow we represent the histogram of the post-correct trials, and in blue the post-error ones. The dashed curves of the corresponding color corresponds to the cumulative functions of these distributions. The corollary discharge is $I_{CD,max} = 0.035$ nA.

However, we observe a decrease of PES at very large coherence (Fig. 8.B), but not of PIA (Fig. 10.B). Moreover the decrease of the PIA effect in Figure 8.C does not occur at the same values of parameters as for the PES one.

As stated by Marco-Pallarés et al. (2008), time courses of PES and PIA seem to be dissociable as post-error improvements in accuracy have been observed with longer inter-trial intervals (up to 2250 ms). We investigate the variation with respect to the RSI of PIA in our model (Figure 11). We note that, for long RSIs, the PIA effect is not observed anymore. However as observed in Marco-Pallarés et al. (2008), the PIA effect occurs for longer RSIs than the PES effect (Figure 11.A). In the same way, PIA is more robust with respect to the intensity of the corollary discharge. This is corroborate by the Figure 11-1, which represents PES and PIA effect for $\tau_{CD} = 500$ ms, hence, with a stronger corollary discharge.

Verguts et al. (2011) find that PIA and PES appear to be statistically independent effects, suggesting that at least two post-error processes takes place in parallel. One surprising outcome of our model is that the network shows PIA and PES effects, both resulting from the same underlying dynamics. In addition, in the parameters domain where they both occur, we find that the variations of those effects with respect to the coherence levels are indeed uncorrelated (Pearson correlation test: RSI of 2000 ms and $I_{CD} = 0.035$ nA, $p = 0.37$, RSI of 500 ms and $I_{CD} = 0.035$ nA, $p = 0.58$, $I_{CD} = 0.05$, $p = 0.79$ and $I_{CD} = 0.1$ nA, $p = 0.25$). This non-correlation highlights the complexity of such post-error adjustments.

In order to obtain more insights into the PIA effect, we study the discrimination threshold following an error or a success, with respect to the RSI (Figure 11.C-E). The definition of the *discrimination threshold* is based on the use of a Weibull function commonly used to fit the psychometric curves (Quick, 1974). That is, one writes the performance (mean success rate) as:

$$\text{Perf}(c) = 1 - 0.5 \exp\left(- (c/\alpha)^\beta\right) \quad (10)$$

where α and β are parameters. Then, for $c = \alpha$, $\text{Perf}(c) = 1 - 0.5 \exp(-1) \sim 0.82$. Hence one defines the discrimination threshold as the coherence level at which the subject responds correctly 82% of the time.

In Figure 11.C we represent the distribution of the discrimination threshold for $I_{CD,max} = 0.035$ nA and a RSI of 500 ms. For these parameters, the distributions for the post-error and post-success cases are

highly different (Smirnov-Kolmogorov test: $p < 10^{-20}$). If we increase the RSI (1000 ms for Figure 11.D and 1500 ms for Figure 11.E), we observe that this difference disappears (Smirnov-Kolmogorov test: $p = 0.038$ and $p = 0.4$ respectively). However, we note that the discrimination threshold distribution is wider after an error than after a correct trial. This might result from the wider distribution in the firing rates (or synaptic activities) after error that we discuss in the next section. To our knowledge, this effect has not yet been studied in human/behavioral experiments.

Dynamical analysis

In this section we show how the PES and PIA effects result from the intrinsic properties of the attractor neural network dynamics. To this end, we provide in Figure 12 a semi qualitative and semi quantitative analysis of the dynamics in the phase plane of the system, for several parameters regimes. Let us first explain how each panel (subfigure) is done. Without loss of generality, we assume that the last decision made is R . Repeated and Alternated cases thus correspond to next trial decisions R and L , respectively. The x and y axis are the synaptic activities S_L and S_R , respectively – hence, the losing and winning populations for the first trial.

Considering trajectories with a same state at the time of the first decision, we represent the *average* dynamics from this decision time to the onset of the new stimulus, that is during the relaxation period. This allows to identify clearly the typical neural states at the end of the relaxation period. From the onset of the new stimulus to the next decision, we represent, starting from the end state of the average dynamics, *one typical* trajectory, observed during 500 ms, as if there were no threshold. Decision actually occurs when the trajectory crosses the decision line – this, approximately: because of the noise, there is not a one to one correspondence between a neural activity reaching the decision threshold and a particular value of the associated synaptic activity. Having all the trajectories plotted for a same duration (and not only until the decision time) allows to visually compare the associated reaction times.

A typical trial with a correct decision will lead, at the time of decision, to losing and winning populations with highly different activity rates, hence a synaptic activity S_L far from the threshold value. On the contrary, a typical error trial will show a losing activity not far from the threshold. We can thus represent post-correct trials, respectively post-error trials, by dynamics with initial states having a rather small, respectively large, value of S_L (and in both cases the first trial winning population S_R at threshold value).

First, we consider the parameter regime exhibiting both PES and PIA (Figure 12.A and B). In the repeated case (Fig. 12.A), at the end of the relaxation (that is at the onset of the next stimulus), both post-correct and post-error trials lie into the correct basin of attraction. Hence, the error rates for these trials are similar. However, the neural states reached at the end of the relaxations are different. Compared to the post-error trial, the post-correct state is closer from the boundary of the new attractor associated to decision R , and the corresponding decision will thus be faster. In the alternated case (Fig. 12.B), the states reached at the end of the relaxation period do not lie within the correct basin of attraction. During the decision-making dynamics, the trajectory needs to cross the boundary between the two basins of attraction. The post-correct trials leading to an alternate decision have a rather straight dynamics across the boundary, leading to relatively fast decision times. In contrast, the states at the onset of the stimulus of the post-error trials are close enough to the boundary so that the corresponding trajectories crosses with a smaller angle the basin boundary. This leads to longer reaction times, hence the PES effect. However, for specific realizations of the noise that lead to error trials (Fig. 12-1) the post-error trials dynamics is closer to the boundary. Thus it has a higher probability to fall on the other side of the basin of attraction. Hence, the error rates are lower for post-error trials than post-correct trials and that explains the PIA effect.

The PEQ effect can be understood from the same kind of analysis. As seen previously, this effect occurs mostly at high level of coherence, as for Fig. 12.C and 12.D. We consider first the repeated case (Figure 12.C). Since the coherence level is high, at the end of the relaxation period, both post-correct and post-error trials lie within the correct basin of attraction, far from the basin boundary. The reaction times and error rates of post-correct and post-error trials for repeated decisions are thus similar.

In contrast, the alternated case (Fig. 12.D) exhibits both the PIA and the PEQ effects. The post-error's end of relaxation now is inside the basin of attraction of the alternated choice. Hence, the error rate will be lower than when the ending point is outside this region (post-correct trials). Moreover, the post-correct trials have to cross the boundary (with a dynamic close to the manifold, hence slower), whereas

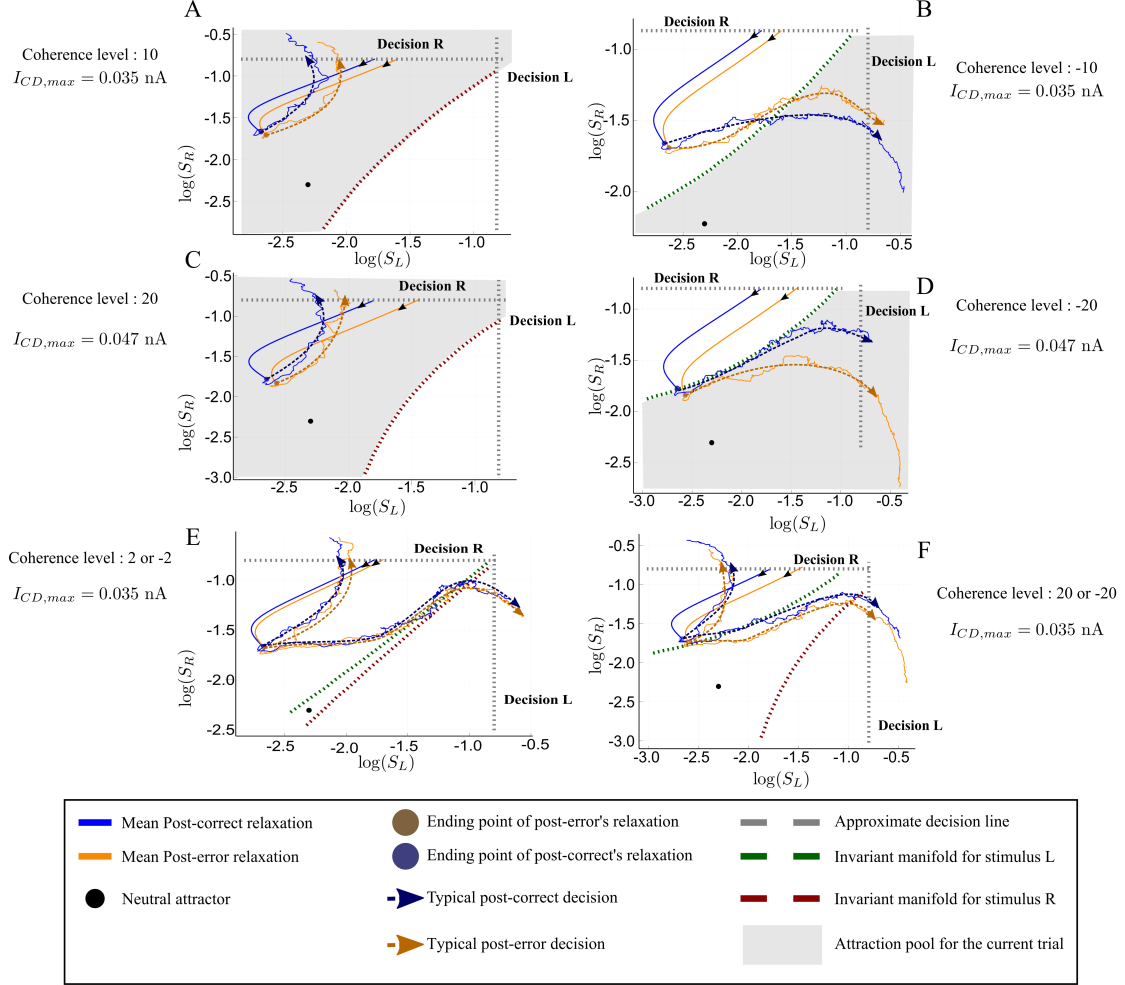


Figure 12: Analysis of the post-error trajectories. Phase-plane trajectories (in log-log plot, for ease of viewing) of the post-correct and post-error trials, for several regimes. We consider that the previous decision was decision R. The black circle shows the neutral attractor state (during the relaxation period). During the presentation of the next stimulus, the attractors and basins of attraction change. (represented by the gray area and the green or red dashed line). Panels (A) and (B): PES and PIA regime ($c = 10$ and $I_{CD,max} = 0.035$ nA). The blue color codes for post-correct trials, and the orange one for post-error. The arrows denote typical time dynamics for (A) repeated decision or (B) alternated decision. For alternated trials, the dynamics needs to cross the invariant manifold (green dashed line), which denotes the boundary between the basins of attraction. Panels (C) and (D): regime with PEQ and PIA ($c = 20$ and $I_{CD,max} = 0.047$ nA). In the alternated case, the post-error relaxation already lies within the alternated basin of attraction. Panel (E): regime without PES or PIA ($c = 2$ and $I_{CD,max} = 0.035$ nA). We show both the alternated and the repeated case, with the corresponding basins of attraction. Panel (F): regime with PIA but without PES ($c = 20$ and $I_{CD,max} = 0.035$ nA). We represent both the alternated and repeated decisions following the relaxation.

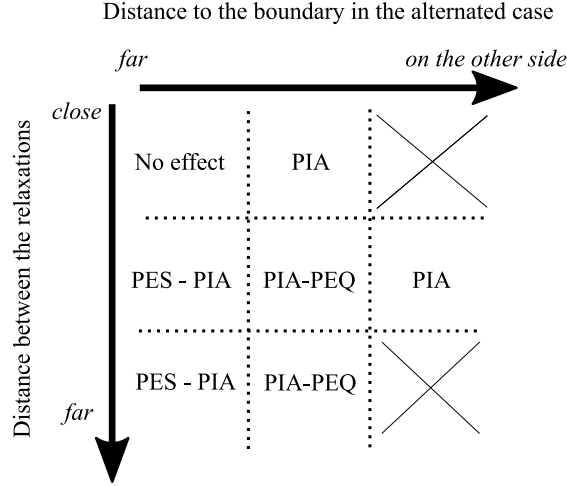


Figure 13: Schematic diagram of the post-error adjustments observations. The x-axis represents the distance between the ending state of the relaxations and the boundary of the following basins of attraction. It goes from "the ending states are far away from the boundary" to "both ending states are in correct basin of attraction". The y-axis corresponds to the distance between the post-error and post-correct relaxations. The crosses denote regions which are not relevant, or inside which the network do not commit errors.

the post-error dynamics can directly reach the new attractor state.

In Figure 12.E we investigate a case, at low coherence level, where neither PIA nor PES is observed. The post-error and post-correct dynamics are very similar and lead to the same relaxation ending point, far from the basin boundary. Finally, in Figure 12.F we consider a case, at high coherence level, where only PIA is observed. Here the relaxations of post-error and post-correct trials are different. However, as for the PEQ effect, at high coherence level both dynamics will be fast. For alternated trials, none of the two ending points are in the correct basin of attraction. Hence, both dynamics need to cross the boundary and have a slow dynamic. The transition in parameter space between no reaction time effect and PEQ effect occurs when the post-error relaxation crosses the basin of attraction of what will be the decision of the next trial.

To conclude, the intrinsic dynamics of the network explain all the post-error adjustments. These post-error adjustments depend on the distributions of the losing and winning populations activities, as the relaxation lead to different states at the onset of the next stimulus. However, it is mainly the relative distances to the boundary between the basins of attraction which explain the variety of effects and their variations with respect to the parameters. We summarize these dependencies in the schematic diagram, Figure 13, even though it does not exhaust the richness of the system's behavior as discussed above.

To gain more insight into the respective influence of the winning and losing population on the post-error adjustments, we compare the synaptic activity distributions. In Table 2 we compare the mean of the post-correct and post-error synaptic activities. We note that, despite the differences in the distributions (see Extended Data Table 2-1 and Table 2-2), the mean activity of the winning population is indistinguishable between post-correct and post-error trials. However, for short RSIs (corresponding to PES regime) the mean synaptic activities of the losing population are different for post-correct and post-error trials.

RSI	Winning Population	Losing Population
500 ms	Fail to reject, $p = 0.16$	Reject, $p = 2.7 \times 10^{-20}$
2000 ms	Fail to reject, $p = 0.87$	Fail to reject, $p = 0.57$

Table 2: Table of the results for Unequal Variance (Welch) test, between the post-error / correct distributions of the firing rates at the time of the decision, with respect to the null hypothesis.

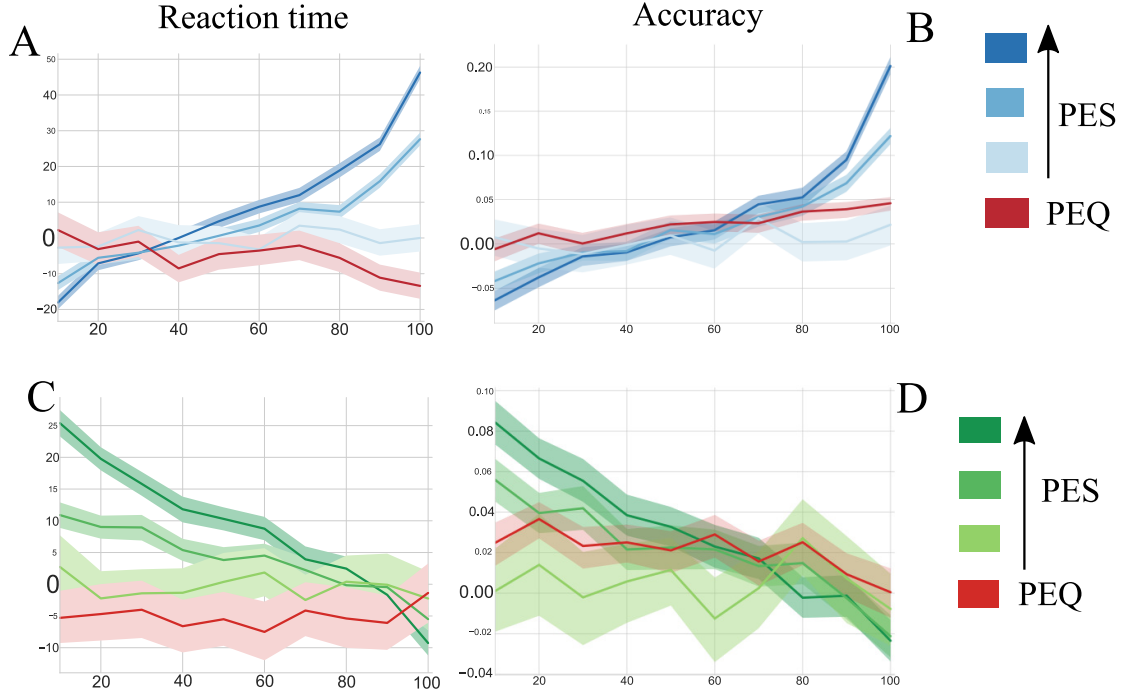


Figure 14: Influence of the losing and winning population on the post-error adjustments. Panels (A) and (B) represents respectively the PES and PIA effect with respect to inter-percentiles range of the losing population synaptic activity distribution, at a RSI of 500 ms. The red curve corresponds to $c = 18$ and $I_{CD,max} = 0.047$, where we observe PEQ. Dark blue corresponds to strong PES effect ($c = 10$, $I_{CD,max} = 0.035$), medium blue to medium PES effect ($c = 5$, $I_{CD,max} = 0.05$). Light blue corresponds to no effect at all ($c = 10$, $I_{CD,max} = 0.035$), for a RSI of 2 seconds. Panels (C) and (D) represent the same curves for the winning population, with the same color code. The shadow area represents the 95% bootstrapped confidence intervals of the corresponding effect.

We further investigate the relative influence on the PES effect of the (previous trial) losing and winning populations. For this, we consider the distributions, at the time of the previous decision, of the synaptic activities of the two populations. In Fig. 14, we plot the amplitude of the PES effect with respect to the inter-percentile range of these distributions. We note that when PES occurs, the higher the activity of the losing population at the time of decision, the stronger this effect will be. The influence of the winning population is observed, although in an opposite way. When PES occurs these effects are correlated (Dark Blue: Pearson correlation: $r = -0.98$ and $p = 2.6 \times 10^{-7}$, Medium Blue: $r = -0.98$ and $p = 9.5 \times 10^{-7}$), in the sense that the variations with respect to the inter-percentile of the winning and losing population are correlated. These observations are coherent with the analysis of the phase-plane trajectories. Indeed, the higher the losing population activity is, the closer to the invariant manifold the state at the end of the relaxation period will be. Hence, the effect will be stronger as it becomes easier (more likely) to cross the boundary.

Furthermore, the dependency in the firing rates for both PES and PIA effects are similar (Figure. 14.C-D), with a stronger effect for high activities of the losing population. This corroborates the above phase plane analysis of the trajectories (Fig. 12). Indeed, the PES and PIA effects both depend on the position of the relaxation in the phase plane. Being closer to the boundary (high activity of the losing population) leads to a smaller error rate at the next trial.

Finally, the dependency of the PEQ effect in the (previous trial) losing and winning populations initial activities is different from the PES one. We can observe an almost constant value of the PES effect with respect to the inter-percentiles of the distributions of the winning and losing populations activities. This is explained by the fact that, in order to observe PEQ, at the end of the error trials relaxation, the network state is in the alternated basin of attraction (if the new stimulus is the opposite one). Hence, the difference between post-correct and post-error dynamics does not depend on how close to the invariant manifold

the corresponding states at the end of the relaxation are, but on which side they are. The PEQ effect does not depend on the losing population activity as the coherence is high enough to result in a strong shift the basin of attraction.

Discussion

In summary, the present work offers a biophysically motivated dynamical framework that is able to capture sequential effects in perceptual decision tasks. We have shown that an attractor neural network accounts, qualitatively and with the correct orders of magnitude, for sequential effects and post-error adjustments reported in experiments, in the absence of any specific feedback about the correctness of the decision. We thus provide evidence that these effects all result from the same intrinsic properties of the neural decision dynamics.

Explanations for post-error slowing

Since the first evidence of PES in behavioral data, several cognitive explanations have been proposed (Rabbitt and Rodgers, 1977; Laming, 1979b,a; Notebaert et al., 2009).

These explanations have been discussed in the framework of drift diffusion models (Ratcliff (1978), Dutilh et al. (2011)). Dutilh et al. (2011) qualify as the most likely effect the hypothesis of *increased response caution*, wherein the response threshold would be modified, the decision becoming less cautious after a correct response and more cautious after an error. These authors do not exclude other mechanisms, notably the *a priori bias* origin. They show that post-error and post-correct trials can be fitted by drift-diffusion models with different starting points. Yet, the neural correlates, which would determine the threshold in the first case, the starting point in the second case, remain quite obscure, especially in the absence of explicit feedback on the correctness of the trial. Within the framework of attractor networks, the sequential effects in choice repetitions are explained by a starting bias, as discussed in Bonaiuto et al. (2016); Gao et al. (2009) and in the present paper. However, we have shown here that post-error adjustments, in the absence of explicit knowledge that an error occurred, result not only from a starting bias, but also from more complex properties of the neural decision dynamics.

Working memory and Decision-Making

In this article we have considered a specific decision-making task: the *free response time task* (Roitman and Shadlen, 2002). In such a task, the subject must make a decision as soon as possible. In the different protocol called *delayed visual motion discrimination experiment* (Shadlen and Newsome, 2001), the subject must make the decision at a prescribed time after the onset of the stimulus. In such task, the decision choice must be stored in order to be retrieved at the prescribed instant of time. In the original model of attractor neural network (Wang (2002), Wong and Wang (2006)), the decision is stored as in a working memory. The persistent activity has been showed to be maintained during several seconds. The implementation of the corollary discharge that we have introduced prevents the model to show working memory effect, which is the price to pay in order to deal with successive decisions with a free response time task. A more complex model of working memory and decision-making has been studied in Murray et al. (2017). This complex architecture has two interacting modules, one implementing the working memory, the other one the decision network. It will be interesting to extend the present work by adding a working memory module in line with Murray et al. (2017), in order to obtain a network performing sequential decision-making while keeping the working memory behavior.

First and higher order sequential effects

Sequential effects can be categorized as first order (if caused by the immediately previous trial), or higher order (if caused by earlier trials in the sequence). The higher order effects of post-error trials have been described for instance in Laming (1979b); Soetens et al. (1984); Cho et al. (2002). The literature discusses several hypotheses on their origin: attention mechanisms, competing motor programs (McPeck et al., 2000), guessing strategies, maintaining or switching, priming or procedural learning (Tipper (2001); Gupta and Cohen (2002)).

To account for such higher order effects, Gao et al. (2009) have introduced a dynamical network composed of four interacting modules. One is an attractor decision network based on (Usher and McClelland, 2001) (a model more directly related to diffusion models than to biophysical models). The other modules include memory units specific to alternated and repeated successive trials.

In this model, even the first order effects result from a coupling between a short-term memory module and the decision network. In contrast, we have shown here that a decision attractor network model, without memory units, presents these first order effects as an intrinsic property of the dynamics. However, due to the nature of the dynamics in our model, we do not expect to reproduce higher-order effects. Indeed, we find that for our model, for parameters for which we observe first order sequential effects (RSI of 1.5 second and $I_{CD,max} = 0.035$ nA), the reaction time distributions for a repetition sequence length of 2 or 1 are indistinguishable (Smirnov-Kolmogorov test: $p = 0.28$), as well as for alternated sequence length of 1 or 2 (Smirnov-Kolmogorov test: $p = 0.65$).

Post-error adjustments have also been experimentally observed at higher order (see Laming (1979b)). Similarly, we do not find higher order post-error adjustments in the behavior of our model, as can be seen in Figure 11-2 obtained from a systematic study in the space ($I_{CD,max}$, c). One may ask whether a more complex architecture, taking into account other areas, could account for higher order repetition biases and post-error adjustments effects as resulting from some intrinsic properties of the dynamics, in the absence of specific memory units.

Openings

During behavioral tasks, subjects are not always aware of their mistakes (Yeung and Summerfield, 2012), but do show post-error slowing. One may thus ask why one does not generally become aware that an error has been made, since the neural dynamics is different following an error or a success. As discussed in the present work, these differences in the dynamics are very subtle. The post-error and post-correct firing rates have broad distributions, with some common properties (the same mean for example). The strong overlapping of these distributions (see Fig. 14) makes difficult to infer the correctness of the decision on a single trial basis. Yet, the tails of the post-error synaptic distribution should allow in some cases to infer that an error has been made. It would be interesting to see in behavioral experiments whether the post-error effects can be related to the confidence in one's decision (Wei and Wang, 2015; Insabato et al., 2017).

Our results also suggest to test experimentally the general picture resulting from our analysis, summarized in Fig. 13, and to test specific effects, such as post-error quickening at large coherence level, the properties of the discrimination threshold distribution in PIA, or the specific variations of post-error adjustments with respect to coherence levels.

Conflict of Interest

The authors declare no competing financial interests.

Acknowledgments

We thank Jérôme Sackur, Jean-Rémy Martin and Laurent Bonnasse-Gahot for useful discussions. KB acknowledges a fellowship from the ENS Paris-Saclay.

References

- Abbott, L. F. and Chance, F. S. (2005). Drivers and modulators from push-pull and balanced synaptic input. In *Progress in Brain Research*, volume 149, pages 147–155.
- Ashby, F. (1983). A biased random walk model for two choice reaction times. *Journal of Mathematical Psychology*, 27(3):277–297.
- Benjamin, D. J., Berger, J. O., Johannesson, M., Nosek, B. A., Wagenmakers, E.-J., Berk, R., Bollen, K. A., Brembs, B., Brown, L., Camerer, C., Cesarini, D., Chambers, C. D., Clyde, M., Cook, T. D.,

- De Boeck, P., Dienes, Z., Dreber, A., Easwaran, K., Efferson, C., Fehr, E., Fidler, F., Field, A. P., Forster, M., George, E. I., Gonzalez, R., Goodman, S., Green, E., Green, D. P., Greenwald, A. G., Hadfield, J. D., Hedges, L. V., Held, L., Hua Ho, T., Hoijtink, H., Hruschka, D. J., Imai, K., Imbens, G., Ioannidis, J. P. A., Jeon, M., Jones, J. H., Kirchler, M., Laibson, D., List, J., Little, R., Lupia, A., Machery, E., Maxwell, S. E., McCarthy, M., Moore, D. A., Morgan, S. L., Munafó, M., Nakagawa, S., Nyhan, B., Parker, T. H., Pericchi, L., Perugini, M., Rouder, J., Rousseau, J., Savalei, V., Schönbrodt, F. D., Sellke, T., Sinclair, B., Tingley, D., Van Zandt, T., Vazire, S., Watts, D. J., Winship, C., Wolpert, R. L., Xie, Y., Young, C., Zinman, J., and Johnson, V. E. (2018). Redefine statistical significance. *Nature Human Behaviour*, 2:6–10.
- Bezanson, J., Edelman, A., Karpinski, S., and Shah, V. B. (2014). Julia: A Fresh Approach to Numerical Computing. *SIAM REVIEW*, 59(1):65–98.
- Bliss, D. P. and DESposito, M. (2017). Synaptic augmentation in a cortical circuit model reproduces serial dependence in visual working memory. *PLoS ONE*, 12(12):7–10.
- Bogacz, R. (2009). Optimal decision making theories. In *Handbook of reward and decision making*, pages 375–397. Academic Press.
- Bonaiuto, J. J., De Berker, A., and Bestmann, S. (2016). Response repetition biases in human perceptual decisions are explained by activity decay in competitive attractor models. *eLife*, 5.
- Busemayer, J. R. and Townsend, J. T. (1993). Decision field theory: A dynamics-cognitive approach to decision making in an uncertain environment. *Psychological Review*, 100(3):432–459.
- Cho, R. Y., Nystrom, L. E., Brown, E. T., Jones, A. D., Braver, T. S., Holmes, P. J., and Cohen, J. D. (2002). Mechanisms underlying dependencies of performance on stimulus history in a two-alternative forced-choice task. *Cognitive, Affective and Behavioral Neuroscience*, 2(4):283–299.
- Cohen, M. X. (2009). Unconscious errors enhance prefrontal-occipital oscillatory synchrony. *Frontiers in Human Neuroscience*, 3(November):1–12.
- Compte, a., Brunel, N., Goldman-Rakic, P. S., and Wang, X. J. (2000). Synaptic mechanisms and network dynamics underlying spatial working memory in a cortical network model. *Cerebral cortex (New York, N.Y. : 1991)*, 10(9):910–23.
- Crapse, T. B. and Sommer, M. A. (2009). Corollary discharge circuits in the primate brain Trinity. *Current Opinion in Neurobiology*, 18(6):552–557.
- Danielmeier, C. and Ullsperger, M. (2011). Post-error adjustments. *Frontiers in Psychology*, 2(SEP):1–10.
- Debener, S. (2005). Trial-by-Trial Coupling of Concurrent Electroencephalogram and Functional Magnetic Resonance Imaging Identifies the Dynamics of Performance Monitoring. *Journal of Neuroscience*, 25(50):11730–11737.
- Dutilh, G., Vandekerckhove, J., Forstmann, B. U., Keuleers, E., Brysbaert, M., and Wagenmakers, E.-J. (2011). Testing theories of post-error slowing. *Attention, Perception, & Psychophysics*, 74(2):454–465.
- Efron, B. and Tibshirani, R. J. (1994). *An Introduction to the Bootstrap*. CRC Press.
- Engel, T. A., Chaisangmongkon, W., Freedman, D. J., and Wang, X. J. (2015). Choice-correlated activity fluctuations underlie learning of neuronal category representation. *Nature Communications*, 6.
- Engel, T. A. and Wang, X.-J. (2011). Same or Different? A Neural Circuit Mechanism of Similarity-Based Pattern Match Decision Making. *Journal of Neuroscience*, 31(19):6982–6996.
- Ermentrout, G. B. and Mahajan, A. (2003). *Simulating, Analyzing, and Animating Dynamical Systems: A Guide to XPPAUT for Researchers and Students*, volume 56.

- Fecteau, J. H. and Munoz, D. P. (2003). Exploring the consequences of the previous trial. *Nature Reviews Neuroscience*, 4(6):435–443.
- Finkel, A. S. and Redman, S. J. (1983). The synaptic current evoked in cat spinal motoneurons by impulses in single group Ia axons. *The Journal of Physiology*, 342(1):615–632.
- Gao, J., Wong-Lin, K., Holmes, P., Simen, P., and Cohen, J. D. (2009). Sequential effects in two-choice reaction time tasks: decomposition and synthesis of mechanisms. *Neural computation*, 21(9):2407–36.
- Gehring, W. J. and Fencsik, D. E. (2001). Functions of the medial frontal cortex in the processing of conflict and errors. *The Journal of Neuroscience*, 21(23):9430–9437.
- Gupta, P. and Cohen, N. J. (2002). Theoretical and computational analysis of skill learning, repetition priming, and procedural memory. *Psychological Review*, 109(2):401–448.
- Hester, R., Foxe, J. J., Molholm, S., Shpaner, M., and Garavan, H. (2005). Neural mechanisms involved in error processing: A comparison of errors made with and without awareness. *NeuroImage*, 27(3):602–608.
- Hollander, M., Wolfe, D. A., and Chicken, E. (2014). *Nonparametric statistical methods.*, volume 2. Wiley Series in Probability and Statistics.
- Insabato, A., Pannunzi, M., and Deco, G. (2017). Multiple Choice Neurodynamical Model of the Uncertain Option Task. *PLoS Computational Biology*, 13(1).
- Jentzsch, I. and Dudschig, C. (2009). Why do we slow down after an error? Mechanisms underlying the effects of posterror slowing. *Quarterly Journal of Experimental Psychology*, 62(2):209–218.
- King, J. A., Korb, F. M., von Cramon, D. Y., and Ullsperger, M. (2010). Post-Error Behavioral Adjustments Are Facilitated by Activation and Suppression of Task-Relevant and Task-Irrelevant Information Processing. *Journal of Neuroscience*, 30(38):12759–12769.
- Laming, D. (1979a). Autocorrelation of choice-reaction times. *Acta Psychologica*, 43(5):381–412.
- Laming, D. (1979b). Choice reaction performance following an error. *Acta Psychologica*, 43(3):199–224.
- Lo, C. C. and Wang, X. J. (2006). Cortico-basal ganglia circuit mechanism for a decision threshold in reaction time tasks. *Nature Neuroscience*, 9(7):956–963.
- Marco-Pallarés, J., Camara, E., Münte, T. F., and Rodríguez-Fornells, A. (2008). Neural mechanisms underlying adaptive actions after slips. *Journal of Cognitive Neuroscience*, 20(9):1595–610.
- McPeck, R. M., Skavenski, A. A., and Nakayama, K. (2000). Concurrent processing of saccades in visual search. *Vision Research*, 40(18):2499–2516.
- Murray, J. D., Jaramillo, J., and Wang, X.-J. (2017). Working memory and decision making in a fronto-parietal circuit model. *Journal of Neuroscience*, 37(50):12167–12186.
- Notebaert, W., Houtman, F., Opstal, F. V., Gevers, W., Fias, W., and Verguts, T. (2009). Post-error slowing: An orienting account. *Cognition*, 111(2):275–279.
- Núñez Castellar, E., Kühn, S., Fias, W., and Notebaert, W. (2010). Outcome expectancy and not accuracy determines posterror slowing: ERP support. *Cognitive, Affective and Behavioral Neuroscience*, 10(2):270–278.
- Quick, R. F. (1974). A vector-magnitude model of contrast detection. *Kybernetik*, 16(2):65–67.
- Rabbitt, P. and Rodgers, B. (1977). What does a man do after he makes an error? an analysis of response programming. *Quarterly Journal of Experimental Psychology*, 29(4):727–743.
- Ratcliff, R. (1978). A theory of memory retrieval. *Psychological Review*, 85(2):59–108.

- Ratcliff, R. (2004). A Comparison of Sequential Sampling Models for Two-Choice Reaction Time. Roger Ratcliff Northwestern University Philip L. Smith University of Melbourne. *Psychological Review*, 111(2):333–367.
- Ratcliff, R. and McKoon, G. (2008). The Diffusion Decision Model: Theory and Data for Two-Choice Decision Tasks. *Neural Computation*, 20(4):873–922.
- Rizzo, M. and Székely, G. (2014). Energy: E-statistics (energy statistics). R package version 1.6.2.
- Rizzo, M. L. and Székely, G. J. (2016). Energy distance. *Wiley Interdisciplinary Reviews: Computational Statistics*, 8(1):27–38.
- Roitman, J. D. and Shadlen, M. N. (2002). Response of neurons in the lateral intraparietal area during a combined visual discrimination reaction time task. *Journal of Neuroscience*, 22(21):9475–9489.
- Shadlen, M. N., Hanks, T. D., Churchland, A. K., Kiani, R., and Yang, T. (2006). The Speed and Accuracy of a Simple Perceptual Decision: A Mathematical Primer. *Bayesian Brain: Probabilistic Approaches to Neural Coding*, pages 207–233.
- Shadlen, M. N. and Newsome, W. T. (1996). Motion perception: seeing and deciding. *Proceedings of the National Academy of Sciences of the United States of America*, 93(January):628–633.
- Shadlen, N. N. and Newsome, W. T. (2001). Neural basis of a perceptual decision in the parietal cortex (area lip) of the rhesus monkey. *Journal of Neurophysiology*, 86:1916–1936.
- Shorack, G. R. and Wellner, J. A. (2009). *Empirical processes with applications to statistics*. Siam.
- Soetens, E., Deboeck, M., and Huetting, J. (1984). Automatic aftereffects in two-choice reaction time: A mathematical representation of some concepts. *Journal of Experimental Psychology: Human Perception and Performance*, 10(4):581–598.
- Szekely, G. and Rizzo, M. (2013). Energy statistics: statistics based on distances. *Journal of Statistical Planning and Inference*, 143(8):1249–1272.
- Tipper, S. P. (2001). Does negative priming reflect inhibitory mechanisms? A review and integration of conflicting views. *Quarterly Journal of Experimental Psychology Section A: Human Experimental Psychology*, 54(2):321–343.
- Townsend, J. T. and Ashby, F. G. (1983). *The stochastic modeling of elementary psychological processes*. Cambridge University Press.
- Usher, M. and McClelland, J. L. (2001). The time course of perceptual choice: The leaky, competing accumulator model. *Psychological Review*, 108(3):550–592.
- Verguts, T., Notebaert, W., Kunde, W., and Wühr, P. (2011). Post-conflict slowing: Cognitive adaptation after conflict processing. *Psychonomic Bulletin and Review*, 18(1):76–82.
- Vickers, D. (1979). *Decision processes in Visual Perception*. Academic Press.
- Wang, X.-J. J. (2002). Probabilistic decision making by slow reverberation in cortical circuits. *Neuron*, 36(5):955–968.
- Wei, W. and Wang, X. J. (2016). Inhibitory Control in the Cortico-Basal Ganglia-Thalamocortical Loop: Complex Regulation and Interplay with Memory and Decision Processes. *Neuron*, 92(5):1093–1105.
- Wei, Z. and Wang, X.-J. (2015). Confidence estimation as a stochastic process in a neurodynamical system of decision making. *Journal of Neurophysiology*, 114(1):99–113.
- Wong, K.-F. and Wang, X.-J. (2006). A Recurrent Network Mechanism of Time Integration in Perceptual Decisions. *Journal of Neuroscience*, 26(4):1314–1328.
- Yeung, N. and Summerfield, C. (2012). Metacognition in human decision-making: confidence and error monitoring. *Philosophical Transactions of the Royal Society B: Biological Sciences*, 367(1594):1310–1321.

Extended Data

Figure 1-1

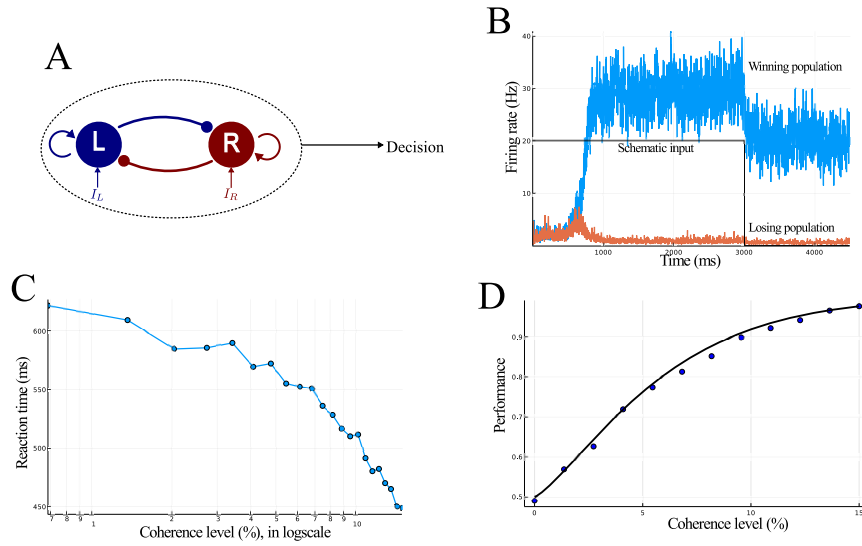


Figure 15: Wong and Wang two-variable model. (A) Reduced two-variable model constituted of two neural units, endowed with self-excitation and effective mutual inhibition. (B) Time course of the two neural activities during a decision-making task. At the beginning the two firing rates are indistinguishable. The firing rate that ramps upward (blue) represents the winning population, the orange one the losing population. A decision is made when one of the firing rate crosses the threshold of 20 Hz. The black line represents the duration of the selective input corresponding to the duration of accumulation of evidence until the decision threshold is reached. This model shows working memory through the persistent activity in the network after the decision is made. Panels (C) and (D), Model simulations on one virtual subject: (C) Mean reaction time in the decision task, and, (D) Performance, both in function of stimulus coherence (stimulus ambiguity).

Figure 1-2

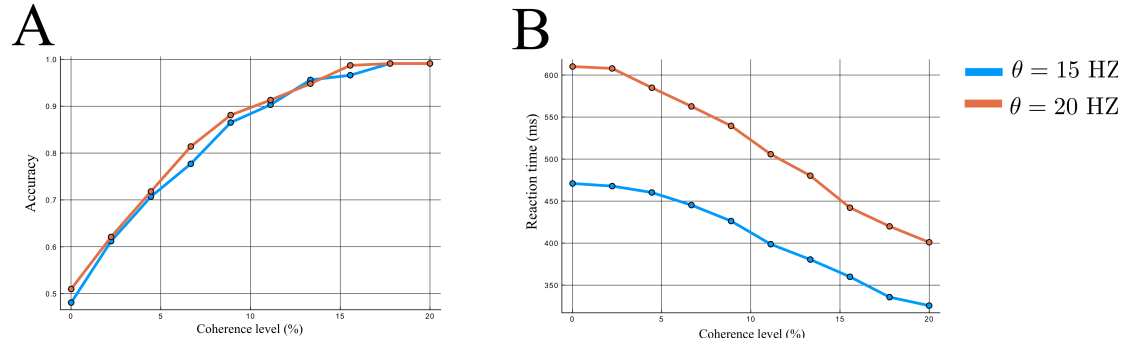


Figure 16: Psychometric and chronometric functions of the original network. (A): Accuracy of the model with respect to coherence levels. In blue we plot the $\theta = 15$ Hz case, and in orange the $\theta = 20$ Hz one. Data are obtained by averaging on 1000 trials. (B) Reaction time of the network, with the same color code. The network still performs decision-making in an analog way to the original model (as the motor reaction time is not taken into account and could be rescaled in a full model).

Figure 1-3

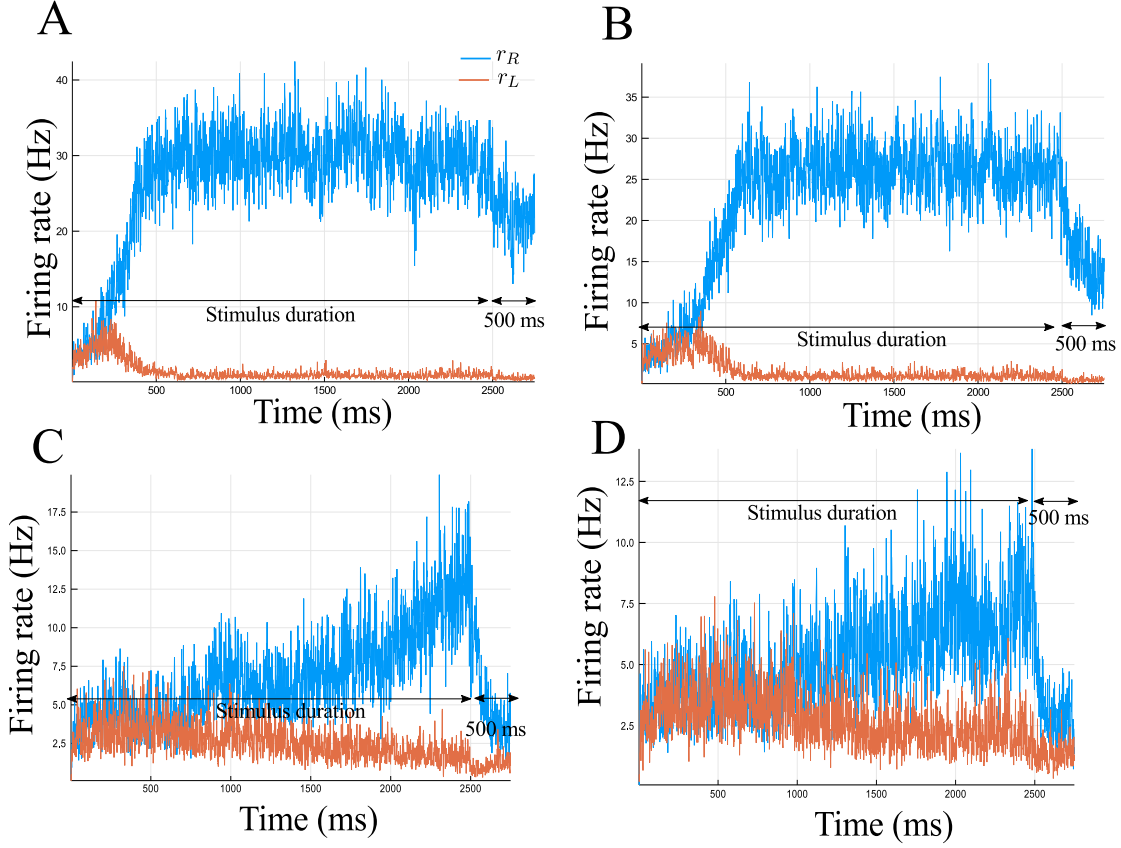


Figure 17: Simulations of the reduced attractor network without the CD input: dynamics with weaker recurrent excitatory weights. We perform simulations of the model with a fixed stimulus duration, and we observe the relaxation during a 500 ms period. Panel (A) corresponds to the original model, which do not show relaxation but working memory. Panel (B) corresponds to a slow relaxation (with $J_{11} = J_{22} = 0.25$), where after 500 ms the system is far from the neutral state. (C) The recurrent excitation is $J_{11} = J_{22} = 0.22$. The state of the system is still highly biased in the favor of the previous choice, and, most importantly, the reaction times are not coherent with behavioral data (more than 2 seconds). (D) The recurrent excitation is $J_{11} = J_{22} = 0.215$. We obtain a relaxation on a time-scale of 500 ms, but the network is not able to perform decision-making anymore as it does not cross the threshold.

Table 1-1

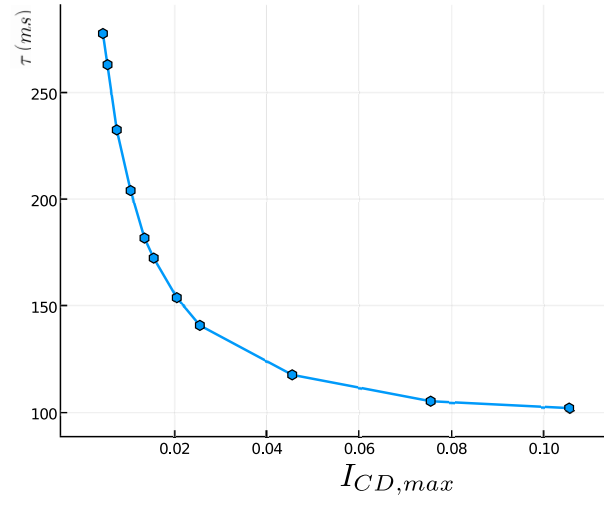
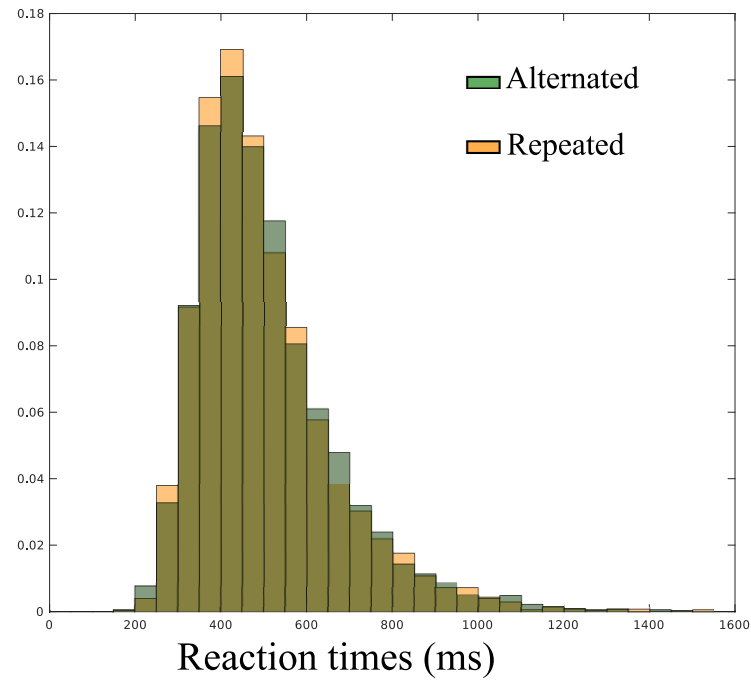


Figure 18: Relaxation time constant. Relaxation time constant of the system during the RSI (that is the relaxation dynamics towards the neutral attractor state), with respect to the corollary discharge amplitude. The values are obtained by computing the eigenvalues of the dynamical system and using the relation $\lambda = \frac{1}{\tau}$, with τ the time constant.

Figure 5-1



*Figure 19: **RSI of 5 seconds.** Histogram of the reaction time for simulations with $I_{CD,max} = 0.035$ nA. The distributions of the reaction times of the two groups are indistinguishable (E-statistic test, $p = 0.61$). The distributions of the coherence levels in these two groups are indistinguishable (Anderson-Darling test: $p = 0.53$).*

Figure 7-1

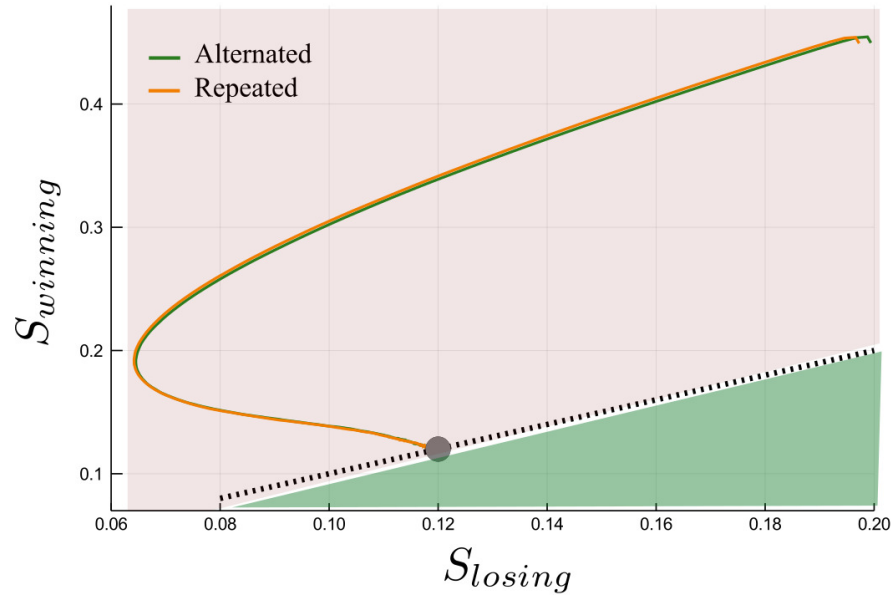
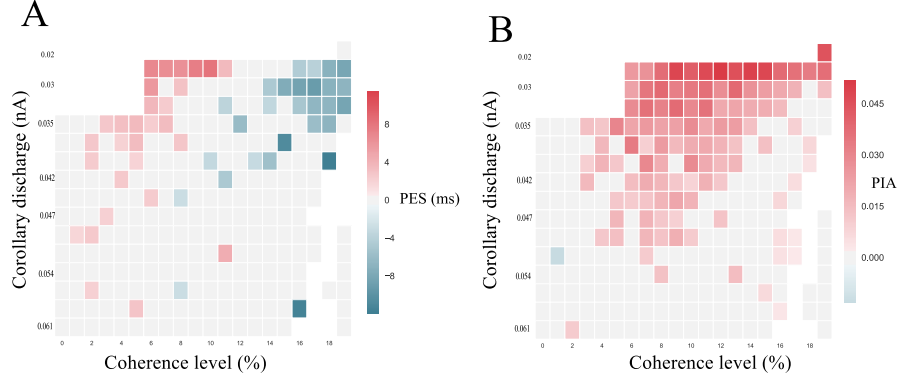


Figure 20: RSI of 5 seconds. Average dynamics between two successive trials in the phase-plane coordinates, during the 500ms preceding the onset of the next stimulus. Anderson-Darling test on the 500 ms prior to stimulus for the synaptic activities: for losing population $p = 0.06$, and for the winning population $p = 0.03$.

Figure 10-1



*Figure 21: **Post-error adjustments at $\tau_{CD} = 500$ ms.** (A) Phase diagram of the PES effect at RSI of 500 ms. The bottom white zone corresponds to parameters where sequential decision-making is impossible. The red square corresponds to regions where PES is observed, and the blue ones where PEQ is observed. We used a bootstrapped confidence interval in order to decide whether or not PES (or PEQ) is observed. (B) Phase diagram of the PIA effect at RSI of 500 ms. The red square corresponds to regions where PIA is observed. We used a bootstrapped confidence interval in order to decide whether or not PIA is observed. The observation of post-error adjustments is highly impacted with the value of τ_{CD} , as we do not observe PES for the same range of parameters.*

Figure 10-2

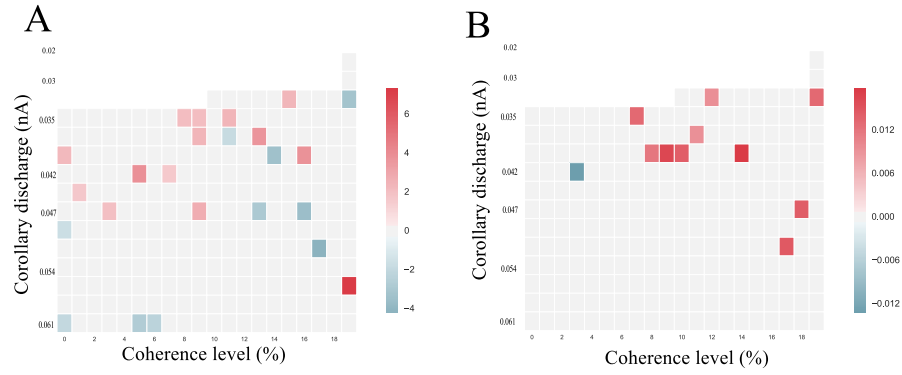


Figure 22: 2nd Order post-error adjustments. (A) Phase diagram of the PES effect at the $n + 2$ trial. (B) Phase diagram of the PIA effect at the $n + 2$ trial. For both panels: Simulations with a RSI of 500 ms, other parameters as in Table 1. The upper white zone corresponds to parameters where sequential decision-making is not possible. Color code as ure 7 (main paper). One sees rare isolated red squares, indicating the absence of any systematic effect.

Figure 12-1

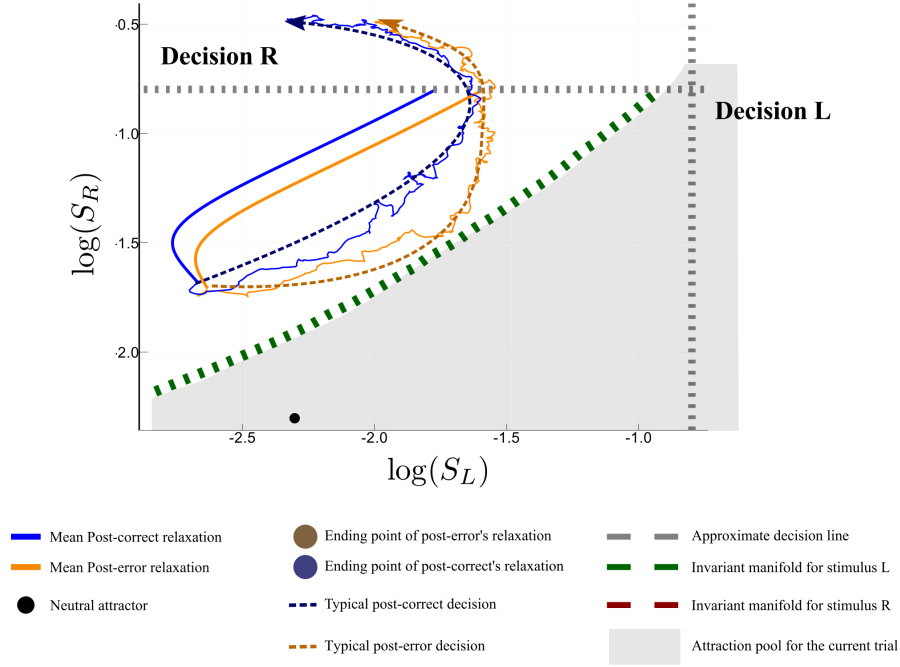


Figure 23: Analysis of the post-error trajectories for error trials. Phase-plane trajectories (in log-log plot, for ease of viewing) of the post-correct and post-error trials, for several regimes. We consider that the previous decision was decision R. The black circle shows the neutral attractor state (during the relaxation period). During the presentation of the next stimulus, the attractors and basins of attraction change. (represented by the gray area and the green or red dashed line). PES and PIA regime ($c = 10$ and $I_{CD,max} = 0.035$ nA). The blue color codes for post-correct trials, and the orange one for post-error. The arrows denote typical time dynamics for error trials when the choice must be L.

Table 2-1

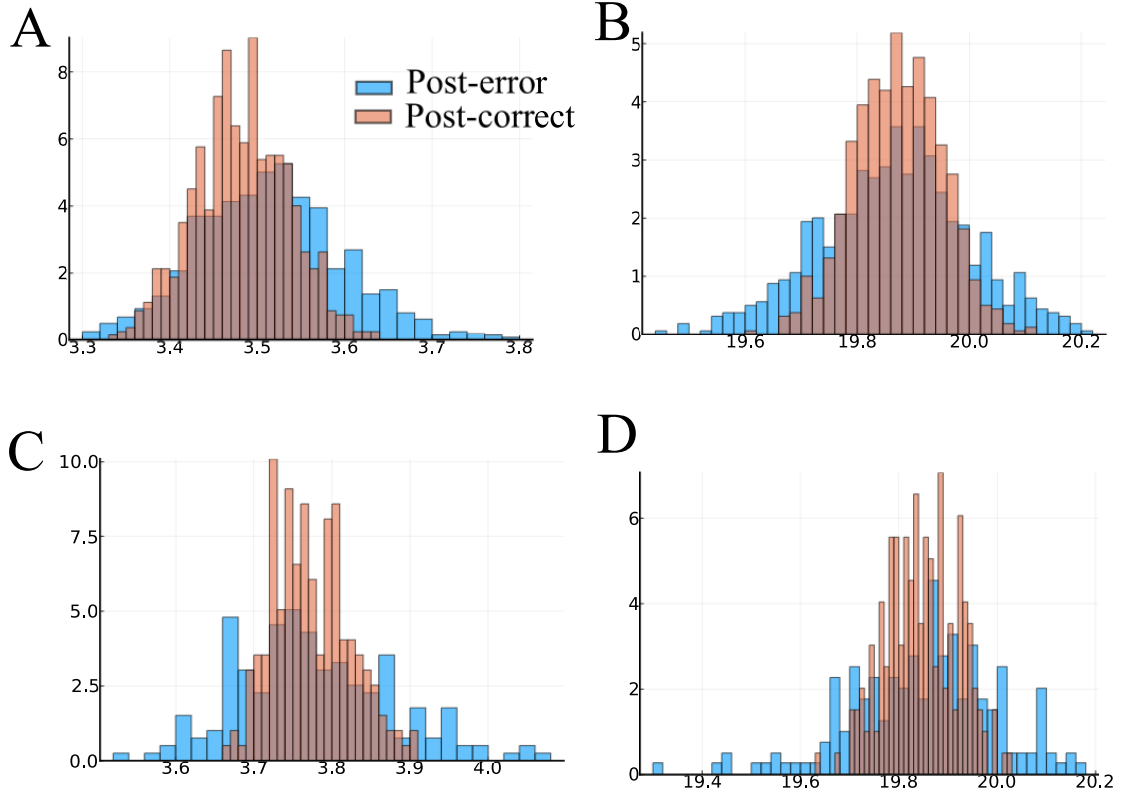


Figure 24: Synaptic distributions at the time of decision. (A) and (C): Distribution of the firing rates, at the time of decision, of the losing population. Each histogram represents a different RSI: 500 ms for (A) and 2000 ms for (C). (B) and (D): Distribution of the firing rates, at the time of decision, of the winning population. Each histogram represents a different RSI: 500 ms for (B) and 2000 ms for (D).

Table 2-2

RSI	Winning Population	Losing Population
500 ms	Reject, $p = 9.9 \times 10^{-8}$	Reject, $p = 5.3 \times 10^{-19}$
2000 ms	Reject, $p = 0.0044$	Reject, $p = 0.00067$

Table 3: Table of the results for the Smirnov-Kolmogorov test between the post-error / correct distributions of the firing rates at the time of the decision, with respect to the null hypothesis.